A THEORETICAL ANALYSIS OF THE TEMPERATURE RESPONSE IN A BIMETALLIC, COMPOSITE GEOMETRY, NUCLEAR REACTOR PRESSURE VESSEL UNDERGOING A LOSS-OF-COOLANT ACCIDENT

by

Lawrence A. Coppari

Dissertation submitted to the Graduate Faculty of the
Virginia Polytechnic Institute and State University
in partial fulfillment of the requirements for the degree of
DOCTOR OF PHILOSOPHY

in

Mechanical Engineering

APPROVED:

J. R. Thomas, Jr., Chairman

J. B. Jones

W. C. Thomas

H. L. Moses

L. W. Johnson

February 1977

Blacksburg, Virginia

Acknowledgements

I wish to express my sincerest gratitude to Dr. James R. Thomas, Jr. for his guidance during my graduate years at Virginia Polytechnic Institute and State University. The author would also like to thank the Mechanical Engineering Department and E. I. duPont de Nemours Company for their financial support. Finally, I wish to extend my thanks to the Computer Center consultants at Burruss Hall for their valuable assistance and to Carolyn Flora for her many hours of excellent typing.

Table of Contents

Table of Contents (Continued)

List of Figures

List of Tables

List of Tables (Continued)

Page

I. Introduction and Literature Search

A problem of current concern in the safety analysis of light water reactors is that of insuring the integrity of the reactor vessel when it is subjected to the thermal shock of emergency cooling injection. The thermal stress developed in the wall is critically dependent upon the temperature gradient of the wall, making accurate time-dependent temperature profiles essential to a stress analysis. Current industry practice [1] utilizes finite difference techniques to solve for the temperature in one dimension, Cartesian geometry ignoring complicating factors such as (1) bimetallic construction, (2) a composite geometry pressure vessel, (3) position variant convective film coefficients at the wetted surface caused by a near stagnation condition of the coolant flow in the lower section, and (4) position and time-dependent internal heat generation within the pressure vessel wall.

It is the purpose of this work to theoretically determine the temperature response of a reactor vessel during a loss of coolant accident to include the aforementioned complicating factors. Thus the endeavor surpasses that which is currently sought in industry. Aside from the in-depth and practical study this work provides, of equal importance to the field of heat transfer are the innovative, steady-state solution derived in Chapter III and the application and evaluation in Chapter IV of the hybrid method to determine two-dimensional transient responses of the pressure vessel.

The analysis of the problem presented herein is divided into three sections. The first, Chapter II, is an analytical solution in one dimension where it is assumed the film coefficient is constant, but the effects of time and position-dependent heat sources are included. The domain of the solution is the wall radius of the upper cylindrical region. A general solution for problems of this type has been given by N. Y. Ölcer [2]. However, in view of the very general character of the solution, it was judged more economical to derive the solution anew. No numerical results are furnished in reference 2.

The third chapter of this work concerns the derivation of the axisymmetric, two-dimensional, steady-state profiles existing in both the cylindrical and hemispherical regions of the vessel prior to the loss of coolant. Until recently, most solutions to the Laplace equation in other than the simplest geometries have been formulated by numerical techniques such as finite difference or finite elements. H. C. Yeh [3] first considered analytical solutions to the Laplace equation in complicated geometries by individually solving for the potential flow in the upper and lower regions of a pressure vessel using the separation of variables method followed by an exploitation of the orthogonality of eigenfunctions to join the two solutions.

In contrast to the potential flow solutions derived in reference 3, a steady-state heat transfer analysis of the pressure vessel by separation of variables requires eigenfunctions that possess the orthogonality characteristic over two regions with differing thermal properties. Sturm-Liouville theory [4] alone gives no insight as to

how to construct this type of eigenfunction. C. W. Tittle [5] was the first to conceive orthogonal expansions which were capable of traversing more than one region through use of discontinuous orthogonality factors constructed from combinations of the thermal properties of each region. Since then, several authors have pursued this subject. Among them were A. C. Giere [6] and M. N. Özisik [7] whose investigations were related to one-dimensional, transient applications. H. C. Yeh [8] addressed the one-dimensional problem of transient heat conduction in a bimetallic reactor pressure vessel and its relation to the orthogonality of eigenfunctions spanning media possessing different thermal properties. However, the solution of reference 8 does not consider internal heat generation.

Because the upper one-half of a pressure vessel is cylindrical and the lower one-half is hemispherical, and moreover because each section generates heat internally by means of absorption of core radiation, two separate coordinate systems are required to adequately describe steady-state heat flow. Clearly, with bimetallic construction and separate coordinate systems, the steady-state analysis essentially requires four, two-dimensional solutions of the Poisson equation. Salient features of the analysis include (1) eigenfunction expansions over bimetallic media, (2) radially dependent but differing internal heat generation in each region of the vessel and (3) the union of the solutions satisfying the inhomogeneous boundary conditions of continuity of heat flux and temperature.

The fourth chapter in the analysis provides the transient,

two-dimensional solution utilizing the temperature profiles derived above as the initial condition for the vessel. The analysis relies on well known techniques such as finite difference and finite elements to approximate the geometry of the vessel. The finite difference set of equations is derived using cylindrical and spherical coordinate systems where appropriate. The finite element solution is derived in Cartesian coordinates and uses a triangular element.

Each of the above approaches results in a set of simultaneous, first order, linear, differential equations. Instead of solving the sets of equations by numerical methods, the sets are solved analytically in time by matrix methods. Such a solution eliminates the need of first obtaining results at early times to determine the temperature distribution at later times. Inherent in a technique such as this are improved accuracy and a lack of stable oscillations induced by numerical procedures. R. Nijsing, and W. Eifler [9] have used this method in conjunction with a finite difference approach handling the spatial variables and have called it the hybrid method. Their work provides a solution to one-dimensional, transient heat flow in fuel rods. The solutions contained in Chapter IV utilize the same approach but in two dimensions for both finite difference and finite element sets of equations. Furthermore, the transient solutions contained herein also consider boiling heat transfer, a topic widely discussed [10,11] and more recently discussed by Burck, Hufschmidt, and de Clercq [12]. In their experimental work, a section of uniformly heated, clad pressure vessel was submersed in a water bath.

Temperature profiles were measured in the wall of the vessel for up to 30 minutes following submersion. It was concluded by their experiments that maximum temperature gradients occur after about eight minutes. The theoretical analysis contained herein also determines the temperature gradients but takes into account an initial non-uniform profile which more closely approximates the actual situation.

II. A One-Dimensional Analysis of the Loss of Coolant Accident

2.1 Statement of the Problem

Reactor vessels are commonly constructed of carbon steel, roughly 0.20 m thick, insulated on the outside and clad on the inside with a thin layer of stainless steel. Since the stainless steel has a thermal conductivity less than half that of carbon steel, it cannot be ignored in a thermal analysis. Thus, the problem is that of solving the time-dependent heat conduction equation in a composite cylinder insulated on the outside, cooled by convection on the inside, and subjected to both time and spatially varying internal heat generation. The vessel is assumed to be at an initial steady-state temperature distribution determined by the heat generated by reactor radiation and by the initial coolant temperature t_0. At time $\Theta = 0$, it is assumed that the coolant temperature drops to t_∞, and the reactor is scrammed, causing the radiation incident upon the vessel to drop suddenly to a lower value, and decrease more slowly thereafter. The vessel temperature $t(r,\Theta)$ for times $\Theta > 0$ is sought.

Labeling the cladding region 1, and the rest of the vessel wall region 2, the governing equation is written as

$$\frac{\partial^2 t}{\partial r^2} + \frac{1}{r}\frac{\partial t}{\partial r} + q_i'''(r,\Theta) = \frac{1}{\alpha_i}\frac{\partial t}{\partial \Theta}, \quad r \in R_i, \quad i = 1,2. \tag{2.1}$$

The energy generation rate may be represented [13] by

$$q_1'''(r,\Theta) = \frac{r_0}{r}\frac{q_0'''}{k_1}\exp[-\mu_1(r - r_0)]\Gamma\Theta^{-p} \tag{2.2a}$$

and

$$q_2'''(r,\Theta) = \frac{r_1}{r}\frac{q_1'''}{k_2}\exp[-\mu_2(r - r_1)]\Gamma\Theta^{-p} \tag{2.2b}$$

where r_0, r_1 and r_2 are the inner radius of the clad and the inner and outer radii of the vessel, respectively; q_0''', q_1''' are the energy generation rates at r_0 and r_1; the k's are the thermal conductivities and the μ's are the radiation attenuation coefficients. The factor $\Gamma\Theta^{-p}$ accounts for the decrease with time of the reactor energy production after shutdown [14]. Also, $\alpha_i = k_i/\rho c_p$, and $(\rho c_p)_1 = (\rho c_p)_2 = \rho c_p$. If $(\rho c_p)_1 \neq (\rho c_p)_2$, a solution by the method that follows is still available [5,6,7].

The boundary conditions to be satisfied by the solution $t(r,\Theta)$ are

$$k_1(\partial t/\partial r)(r_0,\Theta) = h[t(t_0,\Theta) - t_\infty], \quad \Theta > 0. \tag{2.3}$$

$$k_1(\partial t/\partial r)(r_1^-,\Theta) = k_2(\partial t/\partial r)(r_1^+,\Theta), \tag{2.4}$$

$$t(r_1^-,\Theta) = t(r_1^+,\Theta), \tag{2.5}$$

and finally

$$(\partial t/\partial r)(r_2,\Theta) = 0. \tag{2.6}$$

These equations express, respectively, convection to the coolant at the inner boundary, continuity of heat flux and of temperature at

the interface, and insulation at the outer boundary.

In addition to these boundary conditions the solution must satisfy an initial condition which is itself the solution of a boundary value problem

$$t(r,0) = t_0(r), \tag{2.7}$$

where $t_0(r)$ is the solution of the problem obtained by setting $\partial t/\partial\Theta = 0$ in equations (2.1), $p = 0$ in equations (2.2), and $t_\infty = t_0$ in equation (2.3).

2.2 Nondimensionalization

The nondimensional function $w(r,\Theta)$ is defined by

$$w(r,\Theta) = [t(r,\Theta) - t_\infty]/(t_0 - t_\infty). \tag{2.8}$$

By making the additional definitions

$$\bar{r} = \frac{r}{r_2}, \quad a = \frac{r_0}{r_2}, \quad b = \frac{r_1}{r_2}, \quad \xi_i = \mu_i r_2, \quad \Theta = \rho c_p r_2^2 \tau, \quad H = \frac{h r_2}{k_1}, \quad k = \frac{k_2}{k_1},$$

and finally

$$Q_1 = \frac{\Gamma a r_2^2 \, q_0'''\exp(\xi_1 a)}{\Delta t \; k_1} (\rho c_p r_2^2)^{-p}, \quad Q_2 = \frac{\Gamma b r_2^2 \, q_1'''\exp(\xi_2 b)}{\Delta t \; k_2} (\rho c_p r_2^2)^{-p},$$

the problem may be stated in the more concise form

$$\frac{\partial^2 w}{\partial \bar{r}^2} + \frac{1}{\bar{r}} \frac{\partial w}{\partial \bar{r}} + \frac{Q_i \exp(-\xi_i \bar{r})}{\bar{r}} \tau^{-p} = k_i \frac{\partial w}{\partial \tau}, \quad r \in R_i, \quad i = 1,2, \tag{2.9}$$

$$(\partial w/\partial \bar{r})(a,\tau) = Hw(a,\tau), \tag{2.10}$$

$$(\partial w/\partial \bar{r})(b^-,\tau) = k(\partial w/\partial \bar{r})(b^+,\tau), \tag{2.11}$$

$$w(b^-,\tau) = w(b^+,\tau), \tag{2.12}$$

$$(\partial w/\partial \bar{r})(1,\tau) = 0 \tag{2.13}$$

and

$$w(\bar{r},0) = w_0(\bar{r}). \tag{2.14}$$

2.3 Initial Distribution

The initial distribution $w_0(\bar{r})$ is obtained by a straightforward integration of the steady-state equations as described above, so the details will be omitted here.

$$\begin{aligned} w_0(r) = {} & \frac{\bar{Q}_1}{\xi_1}\left[E_1(\xi_1 a) - E_1(\xi_1 r)\right] + \frac{\bar{Q}_1 \exp(-\xi_1 a)}{aH\xi_1} \\ & + \left[\frac{k\bar{Q}_2}{\xi_2}\exp(-\xi_2 b) - \exp(-\xi_2) - \frac{\bar{Q}_1 \exp(-\xi_1 b)}{\xi_1}\right] \\ & \times \left[\frac{1}{aH} + \ln\frac{r}{a}\right] + 1, \quad r \in R_1, \end{aligned} \tag{2.15}$$

and

$$\begin{aligned} w_0(r) = {} & \frac{\bar{Q}_2}{\xi_2}\left[E_1(\xi_2 b) - E_1(\xi_2 r)\right] - \frac{\bar{Q}_2 \exp(-\xi_2)}{\xi_2}\ln\frac{r}{b} \\ & + \frac{\bar{Q}_1}{\xi_1}\left[E_1(\xi_1 a) - E_1(\xi_1 b)\right] + \frac{\bar{Q}_1 \exp(-\xi_1 a)}{aH\xi_1} \\ & + \left[\frac{k\bar{Q}_2}{\xi_2}\left[\exp(-\xi_2 b) - \exp(-\xi_2)\right] - \frac{\bar{Q}_1 \exp(-\xi_1 b)}{\xi_1}\right] \end{aligned}$$

$$x\left[\frac{1}{aH} + \ln\frac{b}{a}\right] + 1, \quad r \in R_2, \tag{2.16}$$

where

$$\bar{Q}_1 = \frac{ar_2^2}{\Delta t\ k_1} q_0'''\exp(\xi_1 a); \qquad \bar{Q}_2 = \frac{br_2^2}{\Delta t\ k_2} q_1'''\exp(\xi_2 b). \tag{2.17}$$

$E_1(x)$ is the exponential integral,

$$E_1(x) = \int_x^\infty \frac{e^{-t}\,dt}{t}, \tag{2.18}$$

and the overbars on the r's have been dropped to simplify notation.

2.4 Solution of the Time-Dependent Problem

Following G.E. Myers [15] the homogeneous problem is considered first and is obtained by deleting the source term. Solutions of the form

$$w(r,\tau) = R(r)\ T(\tau) \tag{2.19}$$

are sought which lead to the ordinary differential equation

$$r^2R''(r) + rR'(r) + \beta_j^2\ r^2R(r) = 0, \qquad j = 1,2, \quad r \in R_j \tag{2.20}$$

for the spatial part of the solution, where

$$\beta_j^2 = k_j\ \beta^2, \tag{2.21}$$

and β is an unknown parameter to be determined. As is well known,

the general solution of equation (2.20) is

$$R(r) = A_j J_0(\beta_j r) + B_j Y_0(\beta_j r), \quad j = 1,2, \quad r \in R_j. \tag{2.22}$$

Applying the boundary conditions given by equations (2.10 - 2.13) to this solution leads to a set of linear homogeneous equations for the constants A_j and B_j, $j = 1,2$. These equations can be written in matrix form as $C(\beta)A = 0$, where

$$C(\beta) = \begin{bmatrix} 0 & 0 & J_1(\beta_2) & Y_1(\beta_2) \\ \beta_1 J_1(\beta_1 a) + H J_0(\beta_1 a) & \beta_1 Y_1(\beta_1 a) + H Y_0(\beta_1 a) & 0 & 0 \\ J_0(\beta_1 b) & Y_0(\beta_1 b) & -J_0(\beta_2 b) & -Y_0(\beta_2 b) \\ \beta_1 J_1(\beta_1 b) & \beta_1 Y_1(\beta_1 b) & -k\beta_2 J_1(\beta_2 b) & -k\beta_2 Y_1(\beta_2 b) \end{bmatrix} \tag{2.23}$$

and $A = [A_1 B_1 A_2 B_2]^T$. Requiring

$$C = \det C = 0 \tag{2.24}$$

yields the eigenvalue condition for determining β. Hence, an infinite sequence of eigensolutions for the homogeneous equation (2.20) is found and is written in the form

$$R_n(r) = \begin{cases} U(\beta_{1n} a)\, J_0(\beta_{1n} r) - Z(\beta_{1n} a)\, Y_0(\beta_{1n} r), & r \in R_1, \\ D_n [Y_1(\beta_{2n})\, J_0(\beta_{2n} r) - J_1(\beta_{2n})\, Y_0(\beta_{2n} r)], & r \in R_2, \end{cases} \tag{2.25}$$

where

$$U(\beta_{1n} a) = \beta_{1n} Y_1(\beta_{1n} a) + H Y_0(\beta_{1n} a), \tag{2.26}$$

$$Z(\beta_{1n}a) = \beta_{1n}J_1(\beta_{1n}a) + HJ_0(\beta_{1n}a), \tag{2.27}$$

and

$$D_n = [U(\beta_{1n}a)J_0(\beta_{1n}b) - Z(\beta_{1n}a)Y_0(\beta_{1n}b)]/$$

$$[Y_1(\beta_{2n})J_0(\beta_{2n}b) - J_1(\beta_{2n})Y_0(\beta_{2n}b)]. \tag{2.28}$$

In equations (2.25 - 2.28) $\beta_{in} = \beta_n\sqrt{k_i}$.

Returning to the inhomogeneous problem, a solution of the form

$$w(r,\tau) = \sum_{n=1}^{\infty} C_n(\tau)R_n(r). \tag{2.29}$$

is attempted. One can prove straightforwardly that the eigenfunctions (2.25) possess the orthogonality property

$$\int_a^1 rR_n(r)R_m(r)\,dr = N_n\,\delta_{mn}, \tag{2.30}$$

where δ_{mn} is the Kronecker delta. Utilizing equation (2.30) to solve for the expansion coefficients $C_n(\tau)$ in equation (2.29),

$$C_n(\tau) = \frac{1}{N_n}\int_a^1 rw(r,\tau)R_n(r)\,dr. \tag{2.31}$$

Again following G. E. Myers [15], equation (2.31) is differentiated with respect to τ, and $\partial w/\partial\tau$ is replaced under the integral with the left-hand side of equation (2.9). This yields

$$\frac{dC_n}{d\tau} = \frac{1}{N_n} \sum_{j=1}^{2} \int_{R_j} \frac{1}{k_j} \left[\frac{\partial}{\partial r} \left(\frac{\partial w}{\partial r} \right) + Q_j \exp(-\xi_j r) \tau^{-p} \right] R_n(r) dr. \qquad (2.32)$$

Integrating by parts twice in equation (2.32) results in the differential equation

$$(dC_n/d\tau) + \beta_n^2 C_n = G_n \tau^{-p}, \qquad (2.33)$$

where

$$G_n = \frac{1}{N_n} \sum_{j=1}^{2} \frac{Q_j}{k_j} \int_{R_j} \exp(-\xi_j r) R_n(r) dr.$$

Equation (2.33) may be integrated straightforwardly to yield the following expression for the expansion coefficients $C_n(\tau)$:

$$C_n(\tau) = G_n \exp(-\beta_n^2 \tau) \int_0^{\tau} s^{-p} \exp(\beta_n^2 s) ds + C_n(0) \exp(-\beta_n^2 \tau). \qquad (2.34)$$

The term $C_n(0)$ can be found from

$$C_n(0) = \frac{1}{N_n} \int_a^1 r w_0(r) R_n(r) dr, \qquad (2.35)$$

with $w_0(r)$ given by equations (2.15) and (2.16). Thus, the complete time-dependent temperature profile is given by equation (2.29), with $R_n(r)$ from equation (2.25) and $C_n(\tau)$ from equation (2.34).

2.5 Results

The infinite series given in equation (2.29) converges quite

rapidly. The temperature profiles for several cases of interest have been computed, but before giving results, the calculational method involved in evaluating equation (2.20) will be briefly mentioned.

First, for a given set of input parameters H, a, b and k, the eigenvalues were computed by Newton's iteration method applied to equation (2.24). It was found that eight eigenvalues were sufficient to give five significant figure accuracy, though 12 eigenvalues were used as a check for short time intervals. The integrals in equations (2.34) and (2.35) were evaluated by Gauss-Legendre quadrature (an elementary transformation was used in equation (2.34) to map the interval $(0,\tau)$ onto $(0,1)$). All reported results were calculated with a 16-point quadrature scheme, although an 80-point scheme was used as a check and found to produce no differences from the values reported. All computations were done in double precision arithmetic on an IBM 370/165 computer. The particular case considered [1] involved a vessel 0.21431 m thick, lined with 0.00476 m stainless steel clad. The original coolant temperature was taken to be $t_0 = 290.8°C$ and the final temperature a conservative $t_\infty = 4.4444°C$, with convection coefficient h = 1988.3 W/m^2-°C. The initial energy generation rate at the water-clad interface was taken to be 258570 W/m^3 [13].

Table 2.1 gives the results of the computations for the initial temperature distribution and for times of 1, 10 and 20 min after initiation of the transient. The results are tabulated as a function of the normalized distance through the wall.

Table 2.1 Time-dependent temperature profiles in a reactor vessel subjected to thermal shock, h = 1988.3 $W/m^2-°C$, b = stainless steel - carbon steel interface.

$\bar{r}$	$\Theta = 0$	$\Theta = 1$ min	$\Theta = 10$ min	$\Theta = 30$ min
0.0	295.6	109.0	49.7	30.2
b	298.1	167.0	75.3	44.7
0.1	300.7	232.1	109.7	64.6
0.2	302.6	279.1	149.6	88.3
0.3	303.6	297.6	184.6	110.2
0.4	304.2	302.9	214.3	129.9
0.5	304.4	304.2	238.4	147.1
0.6	304.6	304.5	257.2	161.5
0.7	304.7	304.6	271.0	172.9
0.8	304.7	304.7	280.4	181.2
0.9	304.7	304.7	285.8	186.2
1.0	304.7	304.7	287.6	187.8

Note that for the conditions chosen, absorption of radiation from the core produces a 9.2°C temperature rise across the wall. Note that this means the outside surface temperature (insulated surface) is 13.9°C higher than it would be if the energy generation were ignored, since then the entire wall would be in equilibrium at the water temperature of 290.8°C. To test the persistence of this effect, the profile was calculated at the same times for $q_0''' = 0$. The results are given in table 2.2. Note that even after 30 min, the outside temperature is still approximately 8.9°C higher with the source than without.

To test the error that might be introduced by treating the problem in slab geometry, a slab geometry solution was constructed. Computed results for the same case considered above differed by less than 1°C from those of the cylindrical geometry solution. However, if the outer radius of the pressure vessel is reduced to 0.91440 with the same wall thickness, a difference of approximately 4% in the outer radius temperature at 30 min exists between cylindrical and slab geometry exact solutions. Table 2.3 illustrates this result. Further reductions in radius yield significant differences between slab and cylindrical geometry solutions.

Tables 2.4 and 2.5 tabulate the time-temperature history for values of h, the convective coefficient, of 8511.7 and 851.17 $W/m^2-°C$ respectively. As anticipated, a coefficient of 8511.7 $W/m^2-°C$ causes large temperature gradients in the wall of the pressure vessel.

Table 2.2 Time-dependent temperature profiles in a reactor vessel with no radiation heating, h = 1988.3 $W/m^2-°C$, b = stainless steel - carbon steel interface.

$\bar{r}$	$\Theta = 0$	$\Theta = 1$ min	$\Theta = 10$ min	$\Theta = 30$ min
0.0	290.8	105.0	47.3	28.6
b	290.8	160.9	71.9	42.4
0.1	290.8	223.3	104.4	61.1
0.2	290.8	268.1	142.3	83.6
0.3	290.8	285.2	175.9	104.4
0.4	290.8	289.8	204.3	123.3
0.5	290.8	290.7	227.4	139.7
0.6	290.8	290.8	245.4	153.6
0.7	290.8	290.8	258.7	164.5
0.8	290.8	290.8	267.7	172.4
0.9	290.8	290.8	272.9	177.2
1.0	290.8	290.8	274.6	178.8

Table 2.3 Time-dependent temperature profiles in a 6 ft diameter reactor vessel subjected to thermal shock, h = 1988.3 $W/m^2-°C$, b = stainless steel - carbon steel interface.

$\bar{r}$	$\Theta = 0$	$\Theta = 1$ min	$\Theta = 10$ min	$\Theta = 30$ min
0.0	295.6	109.8	51.6	32.3
b	298.1	168.1	78.2	48.2
0.1	300.7	233.2	113.6	69.4
0.2	302.5	279.7	154.1	94.4
0.3	303.5	297.7	189.1	117.2
0.4	304.0	302.8	218.4	137.4
0.5	304.3	304.1	241.9	154.7
0.6	304.4	304.3	260.0	169.2
0.7	304.5	304.4	273.2	180.4
0.8	304.6	304.5	282.0	188.5
0.9	304.6	304.6	287.1	193.3
1.0	304.6	304.6	288.7	194.9

Table 2.4 Time-dependent profiles for $h = 8511.7\ W/m^2\text{-}°C$, b = stainless steel - carbon steel interface.

$\bar{r}$	$\Theta = 0$	$\Theta = 1$ min	$\Theta = 10$ min	$\Theta = 30$ min
0.0	295.6	35.1	19.8	10.4
b	298.1	109.1	56.9	24.7
0.1	300.7	196.7	106.7	44.7
0.2	302.6	265.0	162.7	68.6
0.3	303.6	293.6	208.5	90.8
0.4	304.2	302.1	243.3	111.1
0.5	304.6	304.1	267.9	128.8
0.6	304.7	304.5	283.9	143.7
0.7	304.7	304.6	293.7	155.7
0.8	304.7	304.7	299.2	164.3
0.9	304.7	304.7	301.8	169.5
1.0	304.7	304.7	302.6	171.3

Table 2.5 Time-dependent profiles for $h = 851.17\ W/m^2\text{-}°C$, b = stainless steel - carbon steel interface.

$\bar{r}$	Θ = 0 min	Θ = 1 min	Θ = 10 min	Θ = 30 min
0.0	295.6	174.9	97.3	62.6
b	298.1	214.6	118.8	75.8
0.1	300.7	258.5	149.2	95.7
0.2	302.6	288.6	183.1	118.1
0.3	303.6	300.0	211.9	138.6
0.4	304.2	303.3	235.8	156.8
0.5	304.4	304.2	254.9	172.6
0.6	304.6	304.5	269.4	185.7
0.7	304.7	304.6	280.1	196.0
0.8	304.7	304.7	287.1	203.5
0.9	304.7	304.7	291.2	207.9
1.0	304.7	304.7	292.5	209.4

To test the accuracy of conventional numerical techniques the problem was solved by both finite difference [14] and finite element [15] techniques using respective spatial mesh sizes of 0.00771 and 0.01902 m. The results closely approximated the exact analytical solution for an outer pressure vessel radius of 2.3860 m. It is interesting to note that the numerical solutions bracketed the exact solution, the finite difference technique producing lower temperature profiles while the finite element technique produced higher profiles for specified times of 0, 10, and 30 min. It might also be mentioned that the finite element method required the most computer time although it had a spatial mesh 2.47 times as coarse but time step equal to that of the finite difference solution. However, the results more closely approximated the exact solution.

2.6 Nomenclature

A_j = expansion coefficient in equation (2.22) to be evaluated by boundary conditions

a = nondimensional inner radius

B_j = expansion coefficient in equation (2.22) to be evaluated by boundary conditions

b = nondimensional radius of metal interface

$C_n(\tau)$ = time-dependent expansion coefficients defined by equation (2.34)

c_p = specific heat

D_n = term defined by equation (2.28)

E_1 = exponential integral defined by equation (2.18)

G_n = term defined by equation (2.33)

H = Biot number based on pressure vessel outer radius

h = convective coefficient

i,j = subscripts, either 1 or 2

J_m = Bessel function of first kind, order m

k = ratio of conductances, k_2/k_1

k_1, k_2 = conductances of liner and pressure vessel wall, respectively

N_n = norm defined by equation (2.30)

n = subscript, either 1 or 2 unless index of summation

p = exponent for time dependence of heat generation after shutdown

Q_1, Q_2 = nondimensional heat generation rates

$\bar{Q}_1, \bar{Q}_2$ = terms defined by equation (2.17)

$q_1'''(r,\theta)$ = term defined by equation (2.2a)

$q_2'''(r,\theta)$ = term defined by equation (2.2b)

q_0''' = internal heat generation per unit time and volume

$R_n(r)$ = eigenfunctions defined by equation (2.25)

r = radial coordinate

$\bar{r}$ = normalized radial coordinate, r/r_2

r_0 = inner radius

r_1 = metal interface radius

r_2 = outer radius of pressure vessel

t = temperature

t_∞ = injected coolant temperature

t_0 = initial coolant temperature

$U(\beta_{in}a)$ = term defined by equation (2.26)

$w(r,\Theta)$ = nondimensional temperature defined by equation (2.8)

$w_0(r)$ = initial nondimensional temperature defined by equations (2.15-2.18)

Y_m = Bessel function of second kind, order m

$Z(\beta_{in}a)$ = term defined by equation (2.27)

α_i = thermal diffusivity for region i

β = eigenvalue

β_i = term defined by equation (2.21)

Γ = coefficient of heat generation term after shutdown

δ_{mn} = Kronecker delta

ξ_i = nondimensional radiation attenuation coefficient

ρ = density

Θ = time variable

τ = time variable redefined appearing in equation (2.9)

μ = linear attenuation coefficient

Δt = $t_0 - t_\infty$.

III. The Initial Profile in Two Dimensions of a Composite Vessel with Internal Heat Generation

3.1 Statement of the Problem

Reactor vessels are composite in geometry, cylindrical in the upper portion and hemispherical in the lower plenum region. The walls of each region are carbon steel roughly 0.20 m thick and clad on the inside with a thin layer of stainless steel. In addition, the core assembly is supported by a plate several inches thick which decreases the nuclear radiation reaching the lower plenum wall. An accurate profile to be used as an initial condition in a transient analysis of thermal shock should reflect these characteristics. The analysis that follows solves for the steady-state profile by the separation of variables technique, taking the aforementioned characteristics under consideration. The coordinate systems used for the solution are shown in Figure 3.1.

Labeling the cladding of the upper cylindrical and lower hemispherical regions 1c and 1s respectively, and the remainder of the vessel wall regions 2c and 2s, the governing equations [7] for the steady flow of heat may be written as

$$\frac{\partial^2 t_{ic}}{\partial r^2} + \frac{1}{r}\frac{\partial t_{ic}}{\partial r} + \frac{\partial^2 t_{ic}}{\partial z^2} + q'''_{ic}(r) = 0, \quad r \in R_i \ ; \quad i=1,2 \tag{3.1}$$

and

$$\frac{\partial^2 t_{is}}{\partial r^2} + \frac{2}{r}\frac{\partial t_{is}}{\partial r} + \frac{(1-x^2)}{r^2}\frac{\partial^2 t_{is}}{\partial x^2} - \frac{2x}{r^2}\frac{\partial t_{is}}{\partial x} + q'''(r) = 0, \quad r \in R_i, \quad i=1,2 \tag{3.2}$$

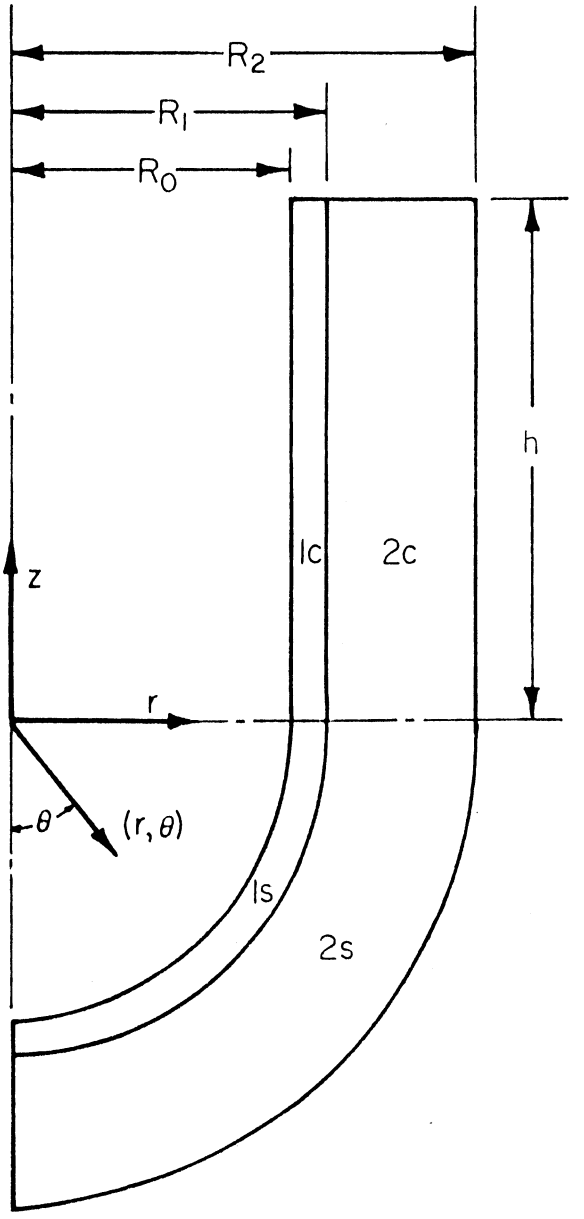

Figure 3.1 Coordinate systems for two-dimensional, initial profile.

where

$$x = \cos\ \theta. \tag{3.2a}$$

The energy generation terms may be represented by

$$q'''_{1c}(r) = \frac{r_o q'''_{oc}}{r k_1} \exp\ [-S_1(r-r_o)],\quad r_o \le r \le r_1, \tag{3.3a}$$

$$q'''_{2c}(r) = \frac{r_o q'''_{oc}}{r k_2} \exp[-S_1(r_1-r_o)]\exp[-S_2(r-r_1)],\ r_1 \le r \le r_2, \tag{3.3b}$$

$$q'''_{1s}(r) = \frac{r_o^2 q'''_{os}}{4\pi k_1 r^2}\exp\ [-S_1(r-r_o)],\quad r_o \le r \le r_1, \tag{3.3c}$$

and

$$q'''_{2s}(r) = \frac{r_o^2 q'''_{os}}{4\pi k_2 r^2} \exp[-S_1(r_1-r_o)]\exp[-S_2(r-r_1)]\ r_1 \le r \le r_2, \tag{3.3d}$$

where r_o, r_1 and r_2 are the inner radius of the clad and the inner and outer radii of the vessel respectively; q'''_{oc} and q'''_{os} are the respective energy generation rates at r_o for the cylindrical and hemispherical regions; the k's are the thermal conductivities, and the S's are the radiation attenuation coefficients. The boundary conditions to be satisfied by the solutions $t_{ic}(r,z)$ and $t_{is}(r,x)$ for i=1,2 are:

$$k_1(\partial t_{1c}/\partial r)(r_o,z) = h_c[t_{1c}(r_o,z)- t_\infty],\ 0 \le z \le h; \tag{3.4}$$

$$k_1(\partial t_{1s}/\partial r)(r_o,\theta) = h_s[t_{1s}(r_o,\theta)- t_\infty],\ 0 \le \theta \le \pi/2; \tag{3.5}$$

$$k_1(\partial t_{1c}/\partial r)(r_1,z) = k_2(\partial t_{2c}/\partial r)(r_1,z),\ 0 \le z \le h; \tag{3.6}$$

$$k_1(\partial t_{1s}/\partial r)(r_1,\theta) = k_2(\partial t_{2s}/\partial r)(r_1,\theta),\ 0 \le \theta \le \pi/2; \tag{3.7}$$

$$t_{1c}(r_1,z) = t_{2c}(r_1,z),\quad 0 \le z \le h; \tag{3.8}$$

$$t_{1s}(r_1,\theta) = t_{2s}(r_1,\theta),\quad 0 \le \theta \le \pi/2; \tag{3.9}$$

$$(\partial t_{2c}/\partial r)(r_2,z) = 0,\quad 0 \le z \le h; \tag{3.10}$$

$$(\partial t_{2s}/\partial r)(r_2,\theta) = 0,\quad 0 \le \theta \le \pi/2; \tag{3.11}$$

$$t_{ic}(r,0) = t_{is}(r,\pi/2),\quad i=1,2,\quad r_o \le r \le r_2; \tag{3.12}$$

$$(\partial t_{ic}/\partial z)(r,0) = \frac{1}{r}\left(\frac{\partial t_{is}}{\partial \theta}\right)(r,\pi/2),\ i=1,2,\ r_o \le r \le r_2; \tag{3.13}$$

$$(\partial t_{ic}/\partial z)(r,h) = 0,\quad i=1,2,\quad r_o \le r \le r_2; \tag{3.14}$$

$$(\partial t_{is}/\partial \theta)(r,0) = 0,\quad i=1,2,\quad r_o \le r \le r_2. \tag{3.15}$$

The equations express, respectively, convection to the coolant at the inner radius in both the upper and lower halves of the pressure vessel, continuity of heat flux and temperature within the upper and lower halves, insulation at the outer radius of both sections, continuity of temperature and heat flux between the upper and lower halves of the vessel, and symmetry about the midplane and around the centerline.

3.2 Redimensionalization

Redefining the variables as follows:

$$\Theta_{ic}(r,z) = t_{ic}(r,z) - t_\infty,\quad r \in \mathcal{R}_i\quad i=1,2, \tag{3.16}$$

$$\theta_{is}(r,x) = t_{is}(r,x) - t_\infty, \quad r \in R_i \quad i=1,2, \tag{3.17}$$

where t_∞ is the coolant temperature, and making the following definitions:

$$\bar{r} = r/r_2, \quad \bar{z} = z/2h, \quad a = r_o/r_2, \quad b = r_1/r_2;$$

$$\mu_{12} = S_1 r_2, \quad \mu_{22} = S_2 r_2, \quad L = r_2^2/4h^2;$$

$$H_c = h_c r_2/k_1, \quad H_s = h_s r_2/k_1, \quad Q_{1c} = \frac{r_o r_2}{k_1} q'''_{oc} \exp(S_1 r_o);$$

$$Q_{2c} = \frac{r_o r_2 q'''_{oc}}{k_2} \exp\,[-S_1(r_1-r_o)] \exp\,(S_2 r_1),$$

$$Q_{1s} = \frac{r_o^2 q'''_{os}}{4\pi k_1} \exp\,(S_1 r_o),$$

$$Q_{2s} = \frac{r_o^2 q'''_{os}}{4\pi k_2} \exp\,[-S_1(r_1-r_o)] \exp\,(S_2 r_1),$$

the problem may be restated as follows:

$$\frac{\partial^2\theta_{ic}}{\partial\bar{r}^2} + \frac{1}{\bar{r}}\frac{\partial\theta_{ic}}{\partial\bar{r}} + L\frac{\partial^2\theta_{ic}}{\partial\bar{z}^2} + \frac{Q_{ic}}{\bar{r}}\exp(-\mu_{i2}\bar{r}) = 0, \quad r \in R_i \quad i=1,2; \tag{3.18}$$

$$\frac{\partial^2\theta_{is}}{\partial\bar{r}^2} + \frac{2}{\bar{r}}\frac{\partial\theta_{is}}{\partial\bar{r}} + \frac{(1-x^2)}{\bar{r}^2}\frac{\partial^2\theta_{is}}{\partial x^2} - \frac{2x}{\bar{r}^2}\frac{\partial\theta_{is}}{\partial x} + \frac{Q_{is}}{\bar{r}^2}\exp(-\mu_{i2}\bar{r}) = 0,$$

$$r \in R_i \quad i=1,2. \tag{3.19}$$

The boundary conditions now become

$$(\partial\Theta_{ic}/\partial\bar{r})(a,\bar{z}) = H_c\Theta_{ic}(a,\bar{z}), \quad i=1, \quad 0 \le \bar{z} \le 1/2; \tag{3.20}$$

$$(\partial\Theta_{is}/\partial\bar{r})(a,\theta) = H_s\Theta_{is}(a,\theta), \quad i=1, \quad 0 \le \theta \le \pi/2; \tag{3.21}$$

$$k_1(\partial\Theta_{1c}/\partial\bar{r})(b,\bar{z}) = k_2(\partial\Theta_{2c}/\partial\bar{r})(b,\bar{z}), \quad 0 \le z \le 1/2; \tag{3.22}$$

$$k_1(\partial\Theta_{1s}/\partial\bar{r})(b,\theta) = k_2(\partial\Theta_{2s}/\partial\bar{r})(b,\theta), \quad 0 \le \theta \le \pi/2; \tag{3.23}$$

$$\Theta_{1c}(b,\bar{z}) = \Theta_{2c}(b,\bar{z}), \quad 0 \le \bar{z} \le 1/2; \tag{3.24}$$

$$\Theta_{1s}(b,\theta) = \Theta_{2s}(b,\theta), \quad 0 \le \theta \le \pi/2; \tag{3.25}$$

$$(\partial\Theta_{ic}/\partial\bar{r})(1,\bar{z}) = 0, \quad i=2, \quad 0 \le \bar{z} \le 1/2; \tag{3.26}$$

$$(\partial\Theta_{is}/\partial\bar{r})(1,\theta) = 0, \quad i=2, \quad 0 \le \theta \le \pi/2; \tag{3.27}$$

$$\Theta_{ic}(\bar{r},0) = \Theta_{is}(\bar{r},\pi/2), \quad i=1,2, \quad a \le \bar{r} \le 1; \tag{3.28}$$

$$\frac{1}{2h}(\partial\Theta_{ic}/\partial\bar{z})(\bar{r},0) = \frac{1}{r_2\bar{r}}(\partial\Theta_{is}/\partial\theta)(\bar{r},\pi/2), \quad i=1,2 \; a \le \bar{r} \le 1; \tag{3.29}$$

$$(\partial\Theta_{ic}/\partial\bar{z})(\bar{r},1/2) = 0, \quad i=1,2, \quad a \le \bar{r} \le 1; \tag{3.30}$$

$$(\partial\Theta_{is}/\partial\theta)(\bar{r},0) = 0, \quad i=1,2, \quad a \le \bar{r} \le 1; \tag{3.31}$$

3.3 Elimination of Inhomogeneous Heat Generation Terms

Before attempting to separate variables, the dependent variables are redefined to eliminate the inhomogeneous terms in the equations. Henceforth, the use of overbars on $\bar{r}$ and $\bar{z}$ is discontinued to simplify notation.

$$\phi_{ic}(r,z) = \Theta(r,z) + f_{ic}(r), \quad i=1,2, \tag{3.32}$$

$$\phi_{is}(r,\theta) = \theta(r,\theta) + f_{is}(r), \quad i=1,2, \tag{3.33}$$

where the functions $f_{ic}(r)$ and $f_{is}(r)$ satisfy

$$f''_{ic}(r) + \frac{1}{r} f'_{ic}(r) = \frac{-Q_{ic}}{r} \exp(-\mu_{i2} r), \quad i=1,2 \tag{3.34}$$

and

$$f''_{is}(r) + \frac{2}{r} f'_{is}(r) = \frac{-Q_{is}}{r^2} \exp(-\mu_{i2} r), \quad i=1,2, \tag{3.35}$$

and where primes denote ordinary derivatives with respect to r. The solutions of equations (3.34) and (3.35) are found by straightforward integration to be

$$f_{ic}(r) = \frac{Q_{ic}}{\mu_{i2}} \int_{R_i} \frac{\exp}{r} (-\mu_{i2} r)dr + C_{i1c} \ln r + C_{i2c}, \quad i=1,2, \tag{3.36}$$

and

$$f_{is}(r) = \frac{Q_{is}}{\mu_{i2}} \int_{R_i} \frac{\exp}{r^2} (-\mu_{i2} r) - \frac{C_{i1s}}{r} + C_{i2s}, \quad i=1,2. \tag{3.37}$$

Inasmuch as the above solutions contain eight arbitrary constants of integration, the homogeneity of the boundary conditions may be preserved if the eight constants are chosen as

$$C_{21c} = \frac{-Q_{2c}}{\mu_{22}} \exp(-\mu_{22}),$$

$$C_{11c} = \frac{-Q_{1c}}{\mu_{12}} \exp(-\mu_{12} b) + \frac{k_2}{k_1} \left[C_{21c} + \frac{Q_2}{\mu_{22}} \exp(-\mu_{22} b)\right],$$

$$C_{12c} = -C_{11c} \ln a + \frac{1}{H_c} \left[\frac{Q_{1c}}{\mu_{12} a} \exp(-\mu_{12} a) + \frac{C_{11c}}{a} \right],$$

$$C_{22c} = \frac{Q_{1c}}{\mu_{12}} \int_a^b \frac{\exp}{r} (-\mu_{12} r) dr + \ln b \, [C_{11c} - C_{21c}] + C_{12c},$$

$$C_{21s} = \frac{-Q_{2s}}{\mu_{22}} \exp(-\mu_{22}),$$

$$C_{11s} = \frac{-Q_{1s}}{\mu_{12}} \exp(-\mu_{22} b) + \frac{k_2}{k_1} \left[\frac{Q_{2s}}{\mu_{22}} \exp(-\mu_{22b}) + C_{21s} \right],$$

$$C_{12s} = \frac{C_{11s}}{a} + \frac{1}{H_s a^2} \left[\frac{Q_{1s}}{\mu_{12}} \exp(-\mu_{12} a) + C_{11s} \right],$$

and

$$C_{22s} = \frac{Q_{1s}}{\mu_{12}} \int_a^b \frac{\exp(-\mu_{12} r)}{r^2} dr + \frac{1}{b} [C_{21s} - C_{11s}] + C_{12s} .$$

Inserting variable transformations (3.32) and (3.33), the problem now lends itself to variable separation. The transformed homogeneous governing equations are

$$\frac{\partial^2 \phi_{ic}}{\partial r^2} + \frac{1}{r} \frac{\partial \phi_{ic}}{\partial r} + L \frac{\partial^2 \phi_{ic}}{\partial z^2} = 0, \quad r \in R_i, \; i=1,2; \tag{3.38}$$

$$\frac{\partial^2 \phi_{is}}{\partial r^2} + \frac{2}{r} \frac{\partial \phi_{is}}{\partial r} + \frac{(1-x^2)}{r^2} \frac{\partial^2 \phi_{is}}{\partial x^2} - \frac{2x}{r^2} \frac{\partial \phi_{is}}{\partial x} = 0, \; r \in R_i, \; i=1,2. \tag{3.39}$$

The boundary conditions, equations (3.20-3.31), remain the same except Θ_i is now replaced by the new variable, ϕ_i. The homogeneity of the

boundary conditions is preserved by the choice of integration constants.

3.4 Solution by Separation of Variables

Solutions of the forms $\phi_{ic} = R_{ic}(r)Z(z)$ and $\phi_{is} = R_{is}(r)X(x)$ force separation in each case. Inserting them and replacing partial derivatives with ordinary ones, equations (3.38) and (3.39) now appear as

$$\frac{1}{R_{ic}(r)}\frac{d^2R_{ic}(r)}{dr^2} + \frac{1}{rR_{ic}(r)}\frac{dR_{ic}(r)}{dr} = \frac{-L}{Z(z)}\frac{d^2Z(z)}{dz^2} = -\lambda_c^2, \quad i=1,2 \tag{3.40}$$

and

$$\frac{r^2}{R_{is}(r)}\frac{d^2R_{is}(r)}{dr^2} + \frac{2r}{R_{is}(r)}\frac{dR_{is}(r)}{dr} = \frac{-(1-x^2)}{X(x)}\frac{d^2X(x)}{dx^2} + \frac{2x}{X(x)}\frac{dX(x)}{dx} = -\lambda_s, \quad i=1,2 \tag{3.41}$$

whose solutions are [16,17]

$$R_{ic}(r) = A_{ic}\,J_o(\lambda_c r) + B_{ic}Y_o(\lambda_c r), \quad i=1,2, \tag{3.42}$$

and

$$R_{is}(r) = \frac{1}{\sqrt{r}}\,[A_{is}\,\sin(\alpha \ln r) + B_{is}\cos(\alpha \ln r)], \quad i=1,2, \tag{3.43}$$

where

$$\alpha = \sqrt{\lambda_s - 1/4}\ . \tag{3.44}$$

Applying boundary conditions (3.20, 3.22, 3.24, 3.26) and (3.21, 3.23, 3.25, 3.27) respectively to solutions (3.42) and (3.43) leads to two sets of linear homogeneous equations for the constants A_{ic}, B_{ic}, A_{is}, B_{is} (i=1,2). These equations may be written in matrix form as

$$\underset{\sim}{C}(\lambda_c)\underset{\sim}{A} = \underset{\sim}{0} \quad \text{and} \quad \underset{\sim}{C}(\alpha)\underset{\sim}{A} = \underset{\sim}{0},$$

where

$$\underset{\sim}{C}(\lambda_c) = \begin{bmatrix} 0 & 0 & J_1(\lambda_c) & Y_1(\lambda_c) \\ D_1 & D_2 & 0 & 0 \\ J_o(\lambda_c b) & Y_o(\lambda_c b) & -J_o(\lambda_c b) & -Y_o(\lambda_c b) \\ k_1 J_1(\lambda_c b) & k_1 Y_1(\lambda_c b) & -k_2 J_1(\lambda_c b) & -k_2 Y_1(\lambda_c b) \end{bmatrix}, \tag{3.45}$$

and where

$$D_1 = H_c\, J_o(\lambda_c a) + \lambda_c\, J_1(\lambda_c a), \tag{3.45a}$$

$$D_2 = H_c\, Y_o(\lambda_c a) + \lambda_c\, Y_1(\lambda_c a), \tag{3.45b}$$

and

$$\underset{\sim}{A} = [A_{1c},\ B_{1c},\ A_{2c},\ B_{2c}]^T.$$

For the spherical portion,

$$C(\alpha) = \begin{bmatrix} D_3 & D_4 & 0 & 0 \\ \tan(\alpha \ln b) & 1 & -\tan(\alpha \ln b) & -1 \\ 0 & 0 & 1 & -\frac{1}{2\alpha} \\ D_5 & D_6 & D_7 & D_8 \end{bmatrix} \tag{3.46}$$

where

$$D_3 = \frac{1}{\alpha}\tan(\alpha \ln a)\{aH_s + \frac{1}{2}\} - 1, \tag{3.46a}$$

$$D_4 = \frac{1}{\alpha}\{aH_s + \frac{1}{2}\} + \tan(\alpha \ln a), \tag{3.46b}$$

$$D_5 = \frac{-k_1}{2}\tan(\alpha \ln b) + k_1\,\alpha, \tag{3.46c}$$

$$D_6 = \frac{-k_1}{2} - k_1\,\alpha\,\tan(\alpha \ln b), \tag{3.46d}$$

$$D_7 = \frac{k_2}{2}\tan(\alpha \ln b) - k_2\,\alpha, \tag{3.46e}$$

$$D_8 = \frac{k_2}{2} + k_2\,\alpha\,\tan(\alpha \ln b), \tag{3.46f}$$

and

$$\underset{\sim}{A} = [A_{1s},\ B_{1s},\ A_{2s},\ B_{2s}]^T.$$

Requiring $C = \det \underset{\sim}{C} = 0$ yields the conditions for determining λ_c and α. Hence, infinite sequences of eigensolutions are found for equations (3.40) and (3.41). They are written as

$$R_{nc}(r) = \begin{cases} B_{nc}[F_{nc}J_o(\lambda_{nc}r) + Y_o(\lambda_{nc}r)], & r \in R_1 \\ \\ \dfrac{B_{nc}}{G_{nc}}\left[\dfrac{-Y_1(\lambda_{nc})}{J_1(\lambda_{nc})}\ J_o(\lambda_{nc}r) + Y_o(\lambda_{nc}r)\right], & r \in R_2\ , \end{cases} \tag{3.47}$$

where

$$F_{nc} = -\ \frac{\lambda_{nc}Y_1(\lambda_{nc}a) + H_c Y_o(\lambda_{nc}a)}{H_c J_o(\lambda_{nc}a) + \lambda_{nc}J_1(\lambda_{nc}a)}\ , \tag{3.48}$$

$$G_{nc} = \frac{\frac{-Y_1(\lambda_{nc})}{J_1(\lambda_{nc})} J_o(\lambda_{nc}b) + Y_o(\lambda_{nc}b)}{F_{nc} J_o(\lambda_{nc}b) + Y_o(\lambda_{nc}b)} \quad . \tag{3.49}$$

These eigensolutions satisfy the orthogonality relations

$$\sum_{i=1}^{2} \int_{R_i} k_i r \, R_{inc}(r) R_{imc}(r) dr = N_{mc} \, \delta_{mn} \, , \tag{3.50}$$

where δ_{mn} is the Kronecker delta and

$$N_{mc} = \sum_{i=1}^{2} \int_{R_i} k_i r R_{imc}^2(r) \, dr \, . \tag{3.51}$$

The eigensolutions for the lower half are

$$R_{ns}(r) = \begin{cases} \frac{B_{ns}}{\sqrt{r}} [F_{ns} \sin(\alpha_n \ln r) + \cos(\alpha_n \ln r)], & r \in R_i, \\ \frac{B_{ns} G_{ns}}{\sqrt{r}} \quad \frac{F_{ns} \tan(\alpha_n \ln b) + 1}{\frac{1}{2\alpha_n} \tan(\alpha_n \ln b) + 1}, & r \in R_2 \end{cases} \tag{3.52}$$

where

$$F_{ns} = - \frac{\frac{1}{\alpha_n} \{aH_s + \frac{1}{2}\} + \tan(\alpha_n \ln a)}{\frac{1}{\alpha_n} \tan(\alpha_n \ln a) \{aH_s + \frac{1}{2}\} - 1} \, , \tag{3.53}$$

$$G_{ns} = \frac{1}{2\alpha_n} \sin(\alpha_n \ln r) + \cos(\alpha_n \ln r) \, , \tag{3.54}$$

with the orthogonality relation

$$\sum_{i=1}^{2} \int_{R_i} k_i R_{isn}(r) R_{ism}(r) dr = N_{ms} \delta_{mn} , \tag{3.55}$$

where

$$N_{ms} = \sum_{i=1}^{2} \int_{R_i} k_i R_{ims}^2(r) dr . \tag{3.56}$$

The remaining constants, B_{nc} and B_{ns}, will be determined later from boundary conditions (3.28) and (3.29).

Focusing attention briefly on the unsolved portions of the separated equations they may immediately be written as

$$\frac{d^2 Z_n(z)}{dz^2} - \beta_n^2 Z_n(z) = 0 , \tag{3.57}$$

where

$$\beta_n^2 = \lambda_{cn}^2 / L \tag{3.58}$$

and

$$(1-x^2) \frac{d^2 X_n(x)}{dx^2} - 2x \frac{dX_n(x)}{dx} - \lambda_{sn} X_n(x) = 0 , \tag{3.59}$$

where

$$x = \cos \theta . \tag{3.60}$$

The solutions are, after applying boundary conditions (3.30) and (3.31),

$$Z_n(z) = B_{nc}[\exp(\beta_n(z-1)) + \exp(-\beta_n z)] \quad 0 \le z \le 1/2 \tag{3.61}$$

and

$$x_{-\frac{1}{2}+i\alpha n}(\theta) = 1 + \frac{4\alpha_n^2 + 1^2}{2^2}\sin^2\frac{\theta}{2} + \frac{(4\alpha_n^2 + 1^2)(4\alpha_n^2 + 3^2)}{2^2 \cdot 4^2}\sin^4\frac{\theta}{2}$$

$$+ \ldots \ , \qquad 0 \le \theta \le \pi/2 \ . \tag{3.62}$$

The functions $x_{-\frac{1}{2}+i\alpha n}$ are sometimes referred to as conal harmonics [17].

The task which remains is to link the solutions of the upper cylindrical portion to those of the lower hemispherical portion satisfying continuity of temperature and heat flux. Before beginning this, the complete solutions as they exist are listed:

$$t_{ic}(r,z) = \sum_{n=1}^{\infty} B_{nc}R_{icn}(r)Z_n(z) - f_{ic}(r) + t_\infty, \ r \in \mathcal{R}_i,$$

$$i=1,2 \qquad 0 \le z \le 1/2, \quad a \le r \le 1 \ ; \tag{3.63}$$

$$t_{is}(r,x) = \sum_{n=1}^{\infty} B_{ns}R_{isn}(r)X_n(x) - f_{is}(r) + t_\infty, \ r \in \mathcal{R}_i,$$

$$i=1,2 \ ; \quad 0 \le x \le 1, \qquad a \le r \le 1 \ . \tag{3.64}$$

Equations (3.63) and (3.64) are the actual temperature profiles.

There remain two sets of expansion coefficients, B_{nc} (for the cylindrical portion) and B_{ns} (for the hemispherical). In addition, the general solutions given by equations (3.63) and (3.64) have not yet been constrained to satisfy continuity of temperature and heat

flux at their mutual boundary. Proceeding in the usual way, the appropriate expressions for temperature and heat flux are equated along the line $\theta = \pi/2$ (z=0), and weighted inner products are taken with either a cylindrical (R_{icm}) or spherical (R_{ism}) eigenfunction. There results an infinite set of equations for the expansion coefficients [3] which is then truncated at a certain order, consistent with the accuracy desired of the final solution. There are several possible ways of determining the order required to yield a given accuracy; the one chosen was to use as many terms as were necessary to represent the particular solutions, equations (3.36) and (3.37), to the desired accuracy. This is a convenient criterion, because these particular solutions can be computed directly, thus providing a standard of comparison. In all cases it was found that seven terms represented the solution to within 0.5°C, the criterion chosen.

Equating temperature profiles of the two regions, equations (3.63) and (3.64) are multiplied by $rR_{icm}(r)k_i$ and integrated over the intervals (a,b) and (b,1). The constants k_i, the respective conductivities, are the discontinuous weighting functions which guarantee orthogonality over the composite region [7]. Adding the results

$$B_{mc}Z_m(0)\,N_{mc} = k_1\int_a^b r[f_{1c}(r) - f_{1s}(r)]R_{1cm}(r)dr$$

$$+ k_2\int_b^1 r[f_{2c}(r) - f_{2s}(r)]R_{2cm}(r)dr + k_1\int_a^b \sum_{n=1}^{\infty} B_{ns}X_n(0)rR_{1sn}(r)$$

$$\cdot R_{1cm}(r)dr + k_2\int_b^1 \sum_{n=1}^{\infty} B_{ns}X_n(0)rR_{2sn}(r)R_{2cm}(r)dr\ , \qquad (3.65)$$

where

$$N_{mc} = k_1 \int_a^b rR_{1cm}^2(r)dr + k_2 \int_b^1 rR_{2cm}^2(r)dr \ , \tag{3.66}$$

and

$$k_1 \int_a^b rR_{1cn}(r)R_{1cm}(r)dr + k_2 \int_b^1 rR_{2cn}(r)R_{2cm}(r)dr = N_{mc}\delta_{mn}. \tag{3.67}$$

The summation operators and functions $X_n(0)$ may be withdrawn from the integrands leaving

$$\begin{aligned} B_{mc} = \frac{1}{N_{mc}Z_m(0)} \Bigg[& k_1 \int_a^b r[f_{1c}(r) - f_{1s}(r)]\, R_{1cm}(r)dr \\ & + k_2 \int_b^1 r[f_{2c}(r) - f_{2s}(r)]R_{2cm}(r)dr + k_1 \sum_{n=1}^{\infty} B_{ns}X_n(0) \\ & \cdot \int_a^b rR_{1sn}(r)R_{1cm}(r)dr + k_2 \sum_{n=1}^{\infty} B_{ns}X_n(0) \int_b^1 rR_{2sn}(r)R_{2cm}(r)dr \Bigg] . \end{aligned} \tag{3.68}$$

Equating heat fluxes, boundary condition (3.29), another expression for the expansion coefficients, B_{mc}, is developed in terms of summations of B_{ns}. Because the details follow closely those used above, they are omitted.

$$\begin{aligned} B_{mc} = \frac{1}{N_{mc}Z'_m(0)} \Bigg[& k_1 \sum_{n=1}^{\infty} B_{ns}X'_n(0) \int_a^b R_{1sn}(r)R_{1cm}(r)dr \\ & + k_2 \sum_{n=1}^{\infty} B_{ns}X'_n(0) \int_b^1 R_{2sn}(r)R_{2cm}(r)dr \Bigg] , \end{aligned} \tag{3.69}$$

where

$$Z_m'(0) = \frac{1}{2h}\frac{\partial Z_m(z)}{\partial z}, \quad z=0 \tag{3.70}$$

and

$$X_n'(0) = \frac{1}{r_2}\frac{\partial X_n(\theta)}{\partial \theta}, \quad \theta = \pi/2. \tag{3.71}$$

The expressions for B_{mc} now may be equated to form an infinite set of linear inhomogeneous equations for the B_{ns}. To solve, the set is truncated at some prescribed k as discussed above. Once B_{1s}, B_{2s}, ... B_{ks} have been determined, either equation (3.68) or (3.69) may be used to compute B_{1c}, B_{2c}, ... B_{kc}. The simultaneous set of equations for B_{ns} appears as follows:

$$\sum_{n=1}^{k}\left[B_{ns}\left[\frac{X_n(0)}{Z_m(0)}\left(k_1\int_a^b rR_{1sn}(r)R_{1cm}(r)dr + k_2\int_b^1 rR_{2sn}(r)R_{2cm}(r)dr\right)\right.\right.$$

$$\left.\left. - \frac{X_n'(0)}{Z_m'(0)}\left(k_1\int_a^b R_{1sn}(r)R_{1cm}(r)dr + k_2\int_b^1 R_{2sn}(r)R_{2cm}(r)dr\right)\right]\right]$$

$$= \frac{1}{Z_m(0)}\left[k_1\int_a^b r[f_{1s}(r) - f_{1c}(r)]R_{1cm}(r) + k_2\int_b^1 r[f_{2s}(r)-f_{2c}(r)]\right.$$

$$\left.\cdot\, R_{2cm}(r)dr\right], \quad m = 1,2, \ldots k \tag{3.72}$$

The steady-state profile is given by equations (3.63) and (3.64) with $R_{icn}(r)$, $Z_n(z)$, $R_{isn}(r)$, $X_n(x)$, $f_{ic}(r)$ and $f_{is}(r)$ from equations (3.47), (3.61), (3.52), (3.62), (3.36) and (3.37) respectively.

One might well ask why it was elected to take inner products with $R_{icm}(r)$ vice $R_{ism}(r)$ in going from equations (3.63-3.64) to equations (3.65-3.67). The choice was completely arbitrary, and in fact the solution was also constructed using $R_{ism}(r)$ to provide another check; this produced identical results.

3.5 Results

Tables 3.1 and 3.2 show the steady-state temperature profiles for the upper and lower regions of the vessel as a function of normalized radius, normalized height, and angular location. For the case under consideration, the coolant temperature, t_∞, is 290.83°C, and internal heat generation rates are 258570 and 51715 W/m^3 for the upper and lower regions respectively. The wall of the vessel is 0.21431 m thick and is lined with 0.00476 m stainless steel clad [1]. The film coefficient is 1988.3 W/m^2-°C. All computation was performed in double-precision arithmetic on an IBM 370/165 computer. The integrations of equation (3.72) were done numerically by Gauss-Legendre quadrature.

In studying Table 3.1 it is apparent that at z=0.05 and z=0.10 the radial temperature profile reaches a maximum at r=0.5 and 0.6, respectively. This is in conflict with usual results of calculations based on a one-dimensional-conduction model, which always show the maximum at the outer (insulated) surface. Further study reveals that at these r-values there is an even more significant temperature gradient in the Z-direction, indicating heat flow toward the bottom

Table 3.1 Two-dimensional steady-state temperature profile in cylindrical region of reactor vessel, h_c = 1988.3 W/m^2-°C, q'''_{oc} = 258570 W/m^3, b = clad-vessel interface.

$\bar{r}$	z = .00	z = .05	z = .10	z = .15	z = .20	z = .40	z = .60	z = 1.00
0.0	293.12	295.07	295.37	295.47	295.51	295.54	295.54	295.54
b	294.48	297.37	297.83	298.00	298.06	298.10	298.10	298.10
0.1	296.24	300.12	300.89	300.92	301.02	301.07	301.08	301.08
0.2	296.89	301.17	302.16	302.51	302.61	302.69	302.69	302.69
0.3	297.38	301.73	302.92	303.36	303.52	303.62	303.63	303.63
0.4	297.69	301.93	303.31	303.84	304.05	304.18	304.18	304.18
0.5	297.82	301.94	303.49	304.06	304.32	304.46	304.47	304.47
0.6	297.88	301.89	303.53	304.17	304.41	304.57	304.57	304.57
0.7	297.94	301.79	303.53	304.21	304.48	304.64	304.65	304.65
0.8	297.95	301.73	303.51	304.23	304.51	304.68	304.68	304.68
0.9	299.96	301.68	303.49	304.23	304.51	304.69	304.69	304.69
1.0	297.98	301.67	303.49	304.23	304.52	304.69	304.70	304.70

Table 3.2 Two-dimensional steady-state temperature profile in hemispherical region of reactor vessel, h_s = 1988.3 W/m^2-°C, q'''_{os} = 51715 W/m^3, b = clad-vessel interface.

$\bar{r}$	θ=90°	θ=85.5	θ=81.0	θ=72.0	θ=54.0	θ=36.0	θ=18.0	θ=0.0
0.0	293.12	291.32	291.04	290.92	290.91	290.91	290.91	290.91
b	294.48	291.60	291.16	290.97	290.95	290.95	290.95	290.95
0.1	296.24	292.06	291.31	291.04	291.00	291.00	291.00	291.00
0.2	296.89	292.43	291.47	291.07	291.02	291.02	291.02	291.02
0.3	297.38	292.72	291.58	291.10	291.04	291.04	291.04	291.04
0.4	297.69	293.02	291.69	291.12	291.04	291.04	291.04	291.04
0.5	297.82	293.27	291.77	291.13	291.05	291.05	291.05	291.05
0.6	297.88	293.42	291.84	291.14	291.05	291.05	291.05	291.05
0.7	297.94	293.56	291.89	291.14	291.05	291.05	291.05	291.05
0.8	297.95	293.66	291.93	291.15	291.06	291.06	291.06	291.06
0.9	297.96	293.71	291.96	291.16	291.06	291.05	291.05	291.05
1.0	297.98	293.73	291.96	291.16	291.06	291.05	291.05	291.05

of the vessel; thus a maximum in the radial profile is not an inconsistency. It should be noted that a finite difference solution constructed for this problem showed this same effect.

3.6 Nomenclature

A_{ic}, A_{is} = cylindrical and spherical expansion coefficients

a = nondimensional inner radius

B_{ic}, B_{is} = cylindrical and spherical expansion coefficients

b = nondimensional radius of clad-wall interface

C_{ijc}, C_{ijs} = arbitrary constants of solution to equations (3.34) and (3.35)

F_{nc}, F_{ns} = terms defined by equations (3.48) and (3.53)

G_{nc}, G_{ns} = terms defined by equations (3.49) and (3.54)

c = subscript denoting upper cylindrical region

H_c, H_s = Biot numbers for upper and lower regions

h = height of cylindrical portion of vessel

h_c, h_s = convective coefficients

i = subscript, either 1 or 2 or $\sqrt{-1}$ when used in equation (3.62)

j = subscript, either 1 or 2

J_m = Bessel function of first kind, order m

k = integer denoting truncation point of an infinite series

k_i = conductivity of liner or vessel wall

L = ratio of square of vessel height to square of its outer radius

m = integer

N_{mc}, N_{ms} = norms, defined by equations (3.51) and (3.56)

n = index of summation

Q_{ic}, Q_{is} = nondimensional heat generation rates

q'''_{oc}, q'''_{os} = internal heat generation per unit time and volume at r_o

$f_{ic}(r)$, $f_{is}(r)$ = solutions to differential equations (3.34) and (3.35)

$R_{nc}(r)$, $R_{ns}(r)$ = eigenfunctions defined by equations (3.47) and (3.52)

r = radial coordinate

$\bar{r}$ = nondimensional radial coordinate

r_o = inner radius of clad

r_1 = radius of clad-wall interface

r_2 = outer radius of pressure vessel

S_i = radiation attenuation coefficient

s = subscript denoting lower hemispherical region

t_{ic}, t_{is} = steady-state temperature profile

t_∞ = temperature of coolant

$X_n(x)$ = conal harmonics, solution to equation (3.59), defined by equation (3.62)

x = cosine of angle measured from vertical in lower region

Y_m = Bessel function of second kind, order m

z = vertical coordinate in upper region

$\bar{z}$ = nondimensional vertical coordinate

$Z_n(z)$ = solution to equation (3.57) defined by equation (3.61)

α = term defined by equation (3.44)

β = term defined by equation (3.58)

δ_{mn} = Kronecker delta

Θ_{ic}, Θ_{is} = temperature defined by equations (3.16) and (3.17)

θ = angle measured from vertical in lower region

λ_c, λ_s = eigenvalues of cylindrical and spherical regions

μ_{i2} = product of radiation attenuation coefficient and outer radius

ϕ_{ic}, ϕ_{is} = transformed temperature variables defined by equations (3.32) and (3.33)

IV. The Two-Dimensional, Transient Solution

4.1 Statement of the Problem

During normal operation the vessel wall (clad and outer regions) has a nonuniform initial temperature profile due to internal heat generation produced by the absorption of nuclear radiation emanating from the core. This heat generation is dissipated by means of convection to pressurized coolant water. At time $\Theta = 0$, the onset of the transient, there is a drop in the coolant temperature and pressure accompanied by a sudden step increase in film coefficients as the newly injected low pressure coolant locally boils when first contacting the vessel wall. Sometime later, the film coefficients will decrease due to the cooling of the vessel walls and cessation of local boiling.

Before proceeding with the transient analysis, the following comments should be made. Following initiation of the transient, all internal heat generation is assumed zero, a reasonable assumption based on the mathematical expression presented by El Wakil [14] for reactor shutdown. Secondly, due to the near stagnation condition at the bottom of the hemispherical section, the forced convection film coefficient will be assumed smaller than that used in the upper section. Figure 4.1 shows the pressure vessel, its coordinate systems, and boundary conditions.

4.2 Finite Difference Formulation

Evenly distributing nodes throughout the pressure vessel as shown

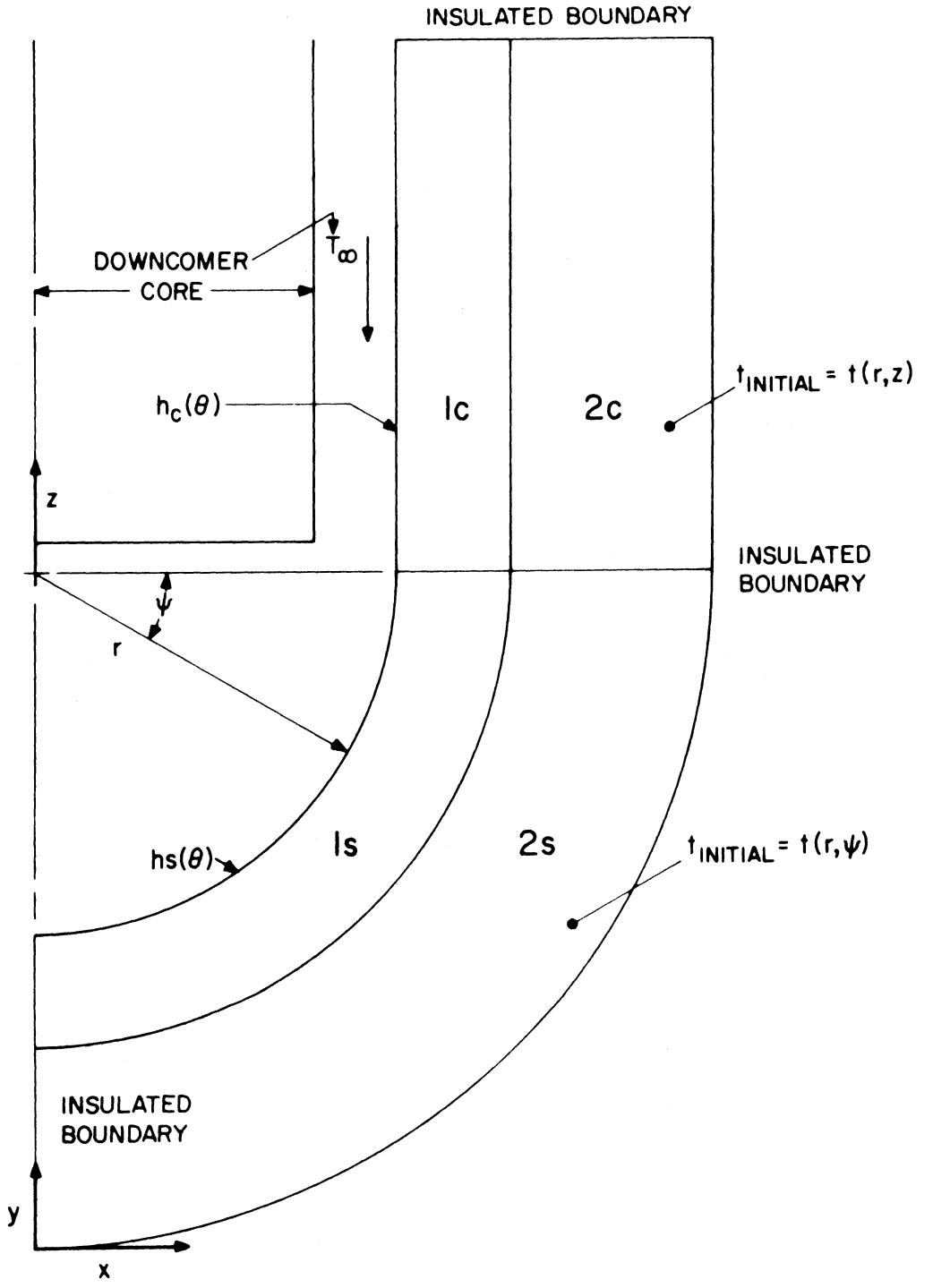

Figure 4.1 Coordinate systems, initial and boundary conditions for two-dimensional, transient solution.

in Fig. 4.2 divides it into a finite number of discrete, ring-shaped volumes. Heat balances are performed on each element, and the results for several typical volumes are given. For a node i, j situated entirely within the carbon steel portion of the cylindrical region, labeled 2C in Fig. 4.1, a heat balance gives

$$-k_2 A^{2C}_{r+\frac{\Delta r}{2}} \frac{(T_{i,j}-T_{i+1,j})}{\Delta r_2} \; -k_2 A^{2C}_{r-\frac{\Delta r}{2}} \frac{(T_{i,j}-T_{i-1,j})}{\Delta r_2} \; -k_2 A^{2C}_{z+\frac{\Delta z}{2}}$$

$$\cdot \frac{(T_{i,j}-T_{i,j+1})}{\Delta z} \; -k_2 A^{2C}_{z-\frac{\Delta z}{2}} \frac{(T_{i,j}-T_{i,j-1})}{\Delta z} = \rho_2 \, C_{\rho 2} \, \Delta V_2$$

$$\cdot \frac{dT_{i,j}}{d\theta} \; . \qquad (4.1)$$

In equation (4.1) ρ_2 and $C_{\rho 2}$ are the respective density and specific heat of node i,j, and Δr_2 and Δz are the radial and vertical dimensions of node i,j respectively. The variable T represents actual node temperatures minus the coolant water temperature (such a change of variables makes the final set of equations homogeneous). Indices i and j denote nodal locations. An increase in i or j causes a corresponding increase in r or z, respectively. The areas through which heat must pass are expressed by

$$A^{2C}_{r\pm\frac{\Delta r}{2}} = 2\pi(r_{i,j} \pm \frac{\Delta r}{2}) \, \Delta z, \qquad (4.2)$$

$$A^{2C}_{z\pm\frac{\Delta z}{2}} = 2\pi \, r_{i,j} \Delta r_2 \qquad (4.3)$$

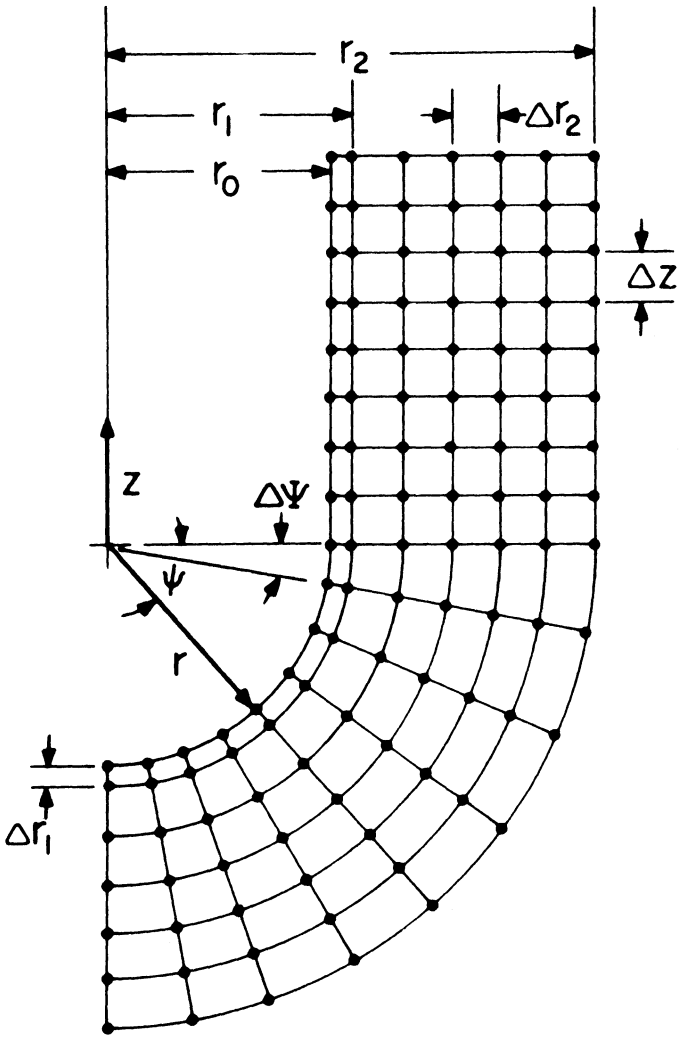

Figure 4.2 Distribution of nodes for finite difference solution.

The volume, ΔV_2, of the element is expressed by

$$\Delta V_2 = 2\pi\, r_{i,j} \Delta z \Delta r_2 \tag{4.4}$$

For a node located entirely within the carbon steel portion of the hemispherical region, labeled 2S, a heat balance leads to

$$-k_2 A^{2S}_{r+\frac{\Delta r}{2}} \frac{(T_{i,j}-T_{i+1,j})}{\Delta r_2} - k_2 A^{2S}_{r-\frac{\Delta r}{2}} \frac{(T_{i,j}-T_{i-1,j})}{\Delta r_2}$$

$$-k_2 A^{2S}_{\psi+\frac{\Delta\psi}{2}} \frac{(T_{i,j}-T_{i,j-1})}{r_{i,j}\Delta\psi} - k_2 A^{2S}_{\psi-\Delta\psi} \frac{(T_{i,j}-T_{i,j+1})}{r_{i,j}\Delta\psi}$$

$$= \rho_2 C_{\rho 2} \Delta V_2 \frac{dT_{i,j}}{d\theta} \tag{4.5}$$

where

$$A^{2S}_{r\pm\frac{\Delta r}{2}} = 2\pi\, (r_{i,j} \pm \frac{\Delta r_2}{2})^2\, \Delta\psi \cos(\psi_{i,j}), \tag{4.6}$$

$$A^{2S}_{\psi\pm\frac{\Delta\psi}{2}} = 2\pi\, r_{i,j} \Delta r_2 \cos(\psi_{i,j} \pm \frac{\Delta\psi}{2}), \tag{4.7}$$

and

$$\Delta V_2 = 2\pi\, r^2_{i,j}\, \Delta r_2 \cos(\psi_{i,j}). \tag{4.8}$$

In this region an increase in i or j causes an increase in r or a decrease in ψ, respectively. A node located at the clad-vessel interface, Fig. 4.3, on the common boundary of the upper and lower regions

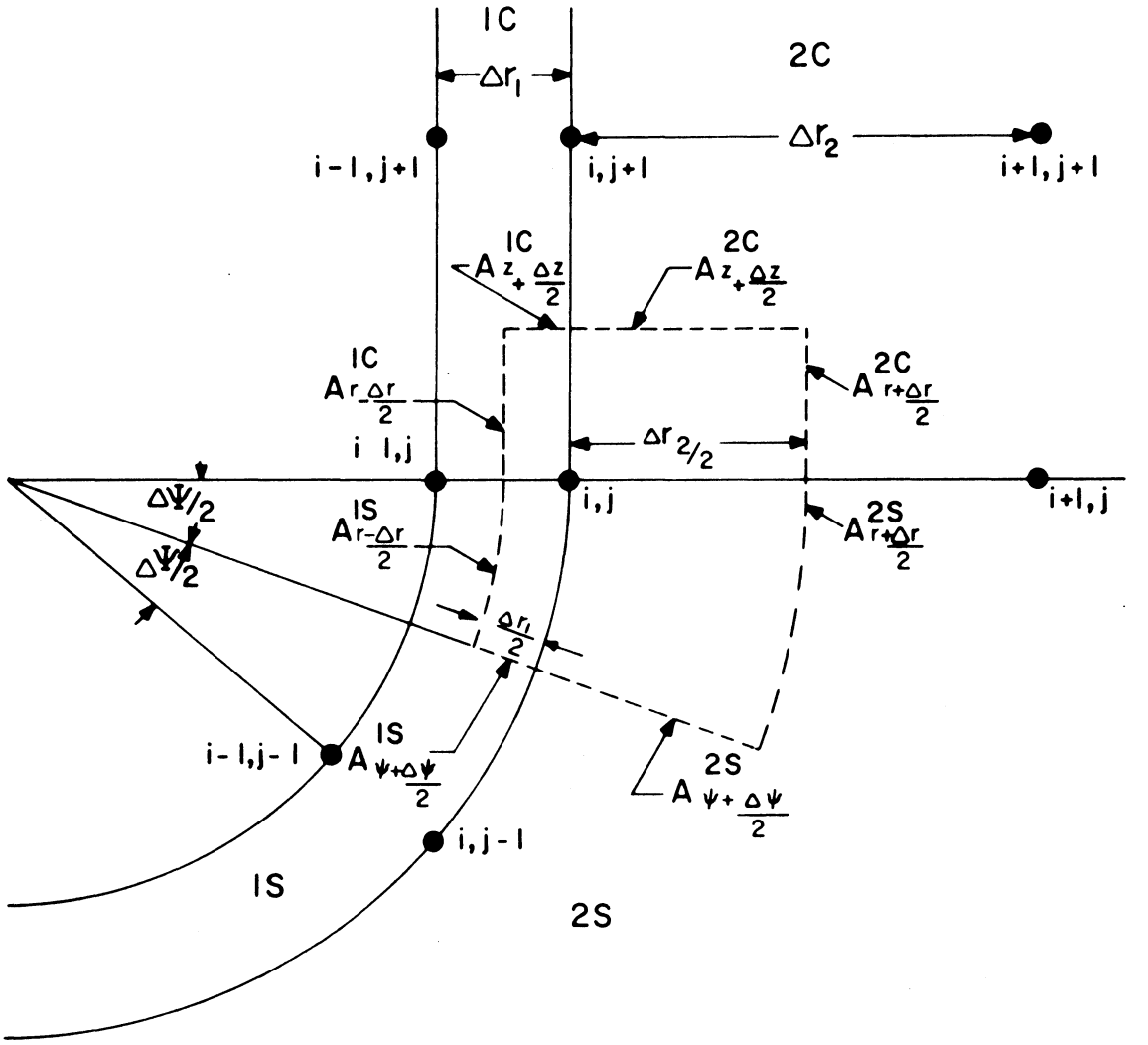

Figure 4.3 Configuration of a node at clad-vessel on common boundary of upper and lower vessel sections.

(where $z = 0$, $\psi = 0$, $r = r_1$) has the following somewhat more complicated nodal equation describing heat transport.

$$-k_2 A^{2C}_{r+\frac{\Delta r}{2}} \frac{(T_{i,j}-T_{i+1,j})}{\Delta r_2} - k_1 A^{1C}_{r-\frac{\Delta r}{2}} \frac{(T_{i,j}-T_{i-1,j})}{\Delta r_1} - k_2 A^{2C}_{z+\frac{\Delta z}{2}} \frac{(T_{i,j}-T_{i,j+1})}{\Delta z}$$

$$-k_2 A^{2S}_{r+\frac{\Delta r}{2}} \frac{(T_{i,j}-T_{i+1,j})}{\Delta r_2} - k_1 A^{1S}_{r-\frac{\Delta r}{2}} \frac{(T_{i,j}-T_{i-1,j})}{\Delta r_1}$$

$$-k_1 A^{1C}_{z+\frac{\Delta z}{2}} \frac{(T_{i,j}-T_{i,j+1})}{\Delta z} \tag{4.9}$$

$$-k_2 A^{2S}_{\psi+\frac{\Delta\psi}{2}} \frac{(T_{i,j}-T_{i,j-1})}{(r_{i,j}+\frac{\Delta r_2}{4})\Delta\psi} = \frac{-k_1 A^{1S}_{\psi+\frac{\Delta\psi}{2}} (T_{i,j}-T_{i,j-1})}{(r_{i,j}-\frac{\Delta r_1}{4})\,\Delta\psi} =$$

$$(\rho_1 C_{\rho 1} \Delta V_1 + \rho_2 C_{\rho 2} \Delta V_2) \frac{d\,T_{i,j}}{d\Theta}$$

where

$$A^{2C}_{r+\frac{\Delta r}{2}} = \pi(r_{i,j}+\frac{\Delta r_2}{2})\,\Delta z, \tag{4.10}$$

$$A^{1C}_{r-\frac{\Delta r}{2}} = \pi(r_{i,j}-\frac{\Delta r_1}{2})\,\Delta z, \tag{4.11}$$

$$A^{2S}_{r+\frac{\Delta r}{2}} = \pi(r_{i,j}+\frac{\Delta r_2}{2})^2\,\Delta\psi\,\cos\frac{\Delta\psi}{4}\,, \tag{4.12}$$

$$A^{1S}_{r-\frac{\Delta r}{2}} = \pi(r_{i,j} - \frac{\Delta r_1}{2})^2 \, \Delta\psi \cos\frac{\Delta\psi}{4} \quad , \tag{4.13}$$

$$A^{2S}_{\psi+\frac{\Delta\psi}{2}} = \pi(r_{i,j} + \frac{\Delta r_2}{4})^2 \, \Delta r_2 \cos\frac{\Delta\psi}{2} \, , \tag{4.14}$$

$$A^{1S}_{\psi+\frac{\Delta\psi}{2}} = \pi(r_{i,j} - \frac{\Delta r_1}{4})^2 \, \Delta r_1 \cos\frac{\Delta\psi}{2} \, , \tag{4.15}$$

$$A^{2C}_{z+\frac{\Delta z}{2}} = \pi(r_{i,j} + \frac{\Delta r_2}{4}) \, \Delta r_2, \tag{4.16}$$

$$A^{1C}_{z+\frac{\Delta z}{2}} = (r_{i,j} - \frac{\Delta r_1}{4}) \, \Delta r_1 \, . \tag{4.17}$$

ΔV_1 and ΔV_2 are the respective volumes associated with the clad and wall portion of the element. They are composite volumes and are expressed as

$$\Delta V_1 = \frac{\pi\Delta r_1}{2} (r_{i,j} - \frac{\Delta r_1}{4}) \, [\Delta z + (r_{i,j} - \frac{\Delta r_1}{4}) \, \Delta\psi \cos\frac{\Delta\psi}{4}], \tag{4.18}$$

$$\Delta V_2 = \frac{\pi\Delta r_2}{2} (r_{i,j} + \frac{\Delta r_2}{4}) \, [\Delta z + (r_{i,j} + \frac{\Delta r_2}{4}) \, \Delta\psi \cos\frac{\Delta\psi}{4}]. \tag{4.19}$$

If a node is located on the wetted boundary at $z = 0$, $\psi = 0$, a mutual point of both regions, a heat balance leads to

$$-h_c A_r^{1C} (T_{i,j}) - h_s A_r^{1S} (T_{i,j} - k_1 A_{z+\frac{\Delta z}{2}}^{1C} \frac{(T_{i,j} - T_{i,j+1})}{\Delta z}$$

$$-k_1 A_{r+\frac{\Delta r}{2}}^{1C} \frac{(T_{i,j} - T_{i+1,j})}{\Delta r_1} - k_1 A_{r+\frac{\Delta r}{2}}^{1S} \frac{(T_{i,j} - T_{i+1,j})}{\Delta r_1}$$

$$-k_1 \frac{A_{\psi+\frac{\Delta\psi}{2}}^{1S} (T_{i,j} - T_{i,j-1})}{(r_{i,j} + \frac{\Delta r_1}{4} \Delta\psi)} = \rho_1 C_{p1} \Delta V_1 \frac{dT_{i,j}}{d\Theta} . \tag{4.20}$$

The areas through which heat passes into and out of the node are expressed by

$$A_r^{1C} = \pi r_{i,j} \Delta z, \tag{4.21}$$

$$A_r^{1S} = \pi r_{i,j}^2 \Delta\psi r_{i,j}^2, \tag{4.22}$$

$$A_{z+\frac{\Delta z}{2}}^{1C} = \pi (r_{i,j} + \frac{\Delta r_1}{4}) \Delta r_1, \tag{4.23}$$

$$A_{r+\frac{\Delta r}{2}}^{1C} = \pi (r_{i,j} + \frac{\Delta r_1}{2}) \Delta z, \tag{4.24}$$

$$A_{r+\frac{\Delta r}{2}}^{1S} = \pi (r_{i,j} + \frac{\Delta r_1}{2})^2 \Delta\psi \cos \frac{\Delta\psi}{4}, \tag{4.25}$$

$$A_{\psi+\frac{\Delta\psi}{2}}^{1S} = \pi (r_{i,j} + \frac{\Delta r_1}{4}) \frac{\Delta r_1}{2} \cos \frac{\Delta\psi}{2} . \tag{4.26}$$

The volume of the element is composite and may be expressed as

$$\Delta V_1 = \frac{\pi \Delta r_1}{2} (r_{i,j} + \frac{\Delta r_1}{4}) [\Delta z + (r_{i,j} + \frac{\Delta r_1}{4}) \Delta\psi \cos \frac{\Delta\psi}{4}]. \tag{4.27}$$

Writing a heat balance for every ring, the set of equations may be expressed in matrix notation as

$$[CAP]\ \{\frac{dT}{d\Theta}\} - [CON]\ \{T\} = \{0\} \tag{4.28}$$

Matrix [CON] is pentadiagonal and symmetric. Matrix [CAP] is diagonal. Both of these characteristics are exploited in the solution technique of Nijsing and Eifler [9].

The actual nodal temperatures are expressed by

$$\{t\} = \{T\} + \{T_\infty\}. \tag{4.29}$$

4.3 Finite Element Formulation

The finite element formulation used in this analysis follows closely that used by Myers [15]. Because the two-dimensional heat capacitance matrix is not constructed in the reference, the details will be supplied. The solution is cast in Cartesian coordinates using triangular elements. Figure 4.4 shows the elemental network.

Beginning with the variational statement for the transient heat equation in Cartesian coordinates, written as

$$VS = \frac{1}{2}\int\int [k\left(\frac{\partial t}{\partial x}\right)^2 + k\left(\frac{\partial t}{\partial y}\right)^2 + \rho\ C_p\ \frac{\partial (t^2)}{\partial \Theta}]\ dxdy, \tag{4.30}$$

a bilinear temperature distribution is assumed within each element for all time. Therefore, the internal temperature of an element may be

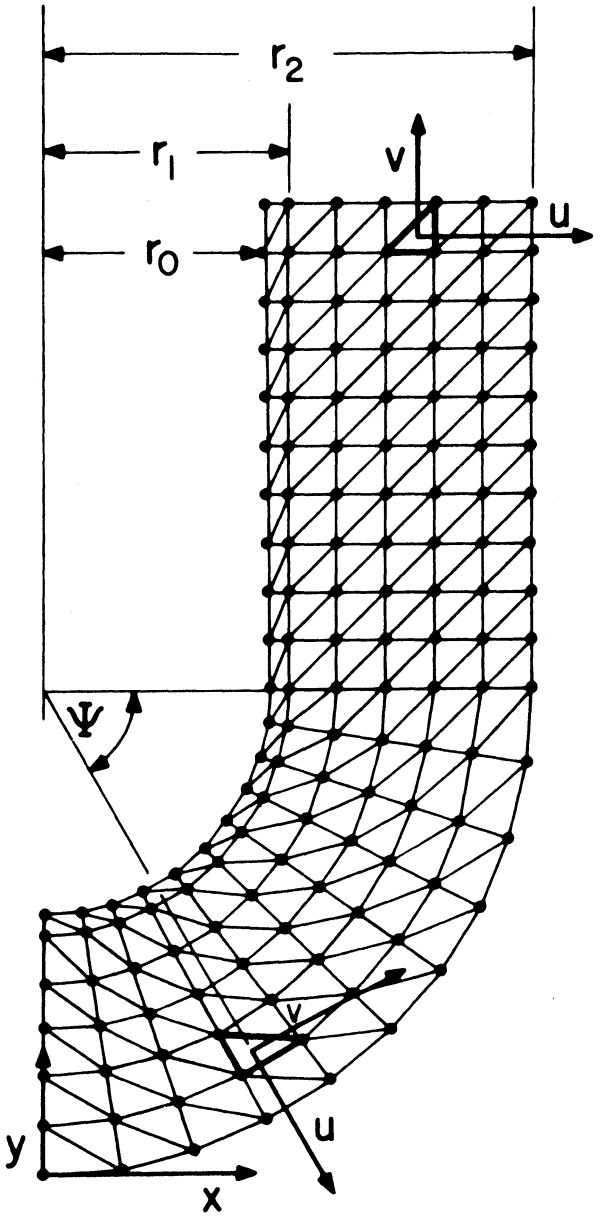

Figure 4.4 Elemental network and coordinate systems for finite element solution.

expressed as

$$\hat{t}^{(e)} = P\, \tilde{R}^{(e)}\, \hat{t}^{(e)} \tag{4.31}$$

where

$$\hat{P}^T = [1 \; x \; y], \tag{4.32}$$

$$\tilde{R}^{(e)} = D \begin{bmatrix} x_j y_k - x_k y_j & x_k y_i - x_i y_k & x_i y_j - x_j y_i \\ -y_{jk} & y_{ik} & -y_{ij} \\ x_{jk} & -x_{ik} & x_{ij} \end{bmatrix}, \tag{4.33}$$

where the scalar D may be expressed

$$D = (x_{ij} y_{jk} - x_{jk} y_{ij})^{-1}, \tag{4.34}$$

and

$$\hat{t}^{(e)} = [t_i \; t_j \; t_k]^T. \tag{4.35}$$

Letters x and y denote the coordinates (whose origin is at the base of the hemisphere) of vertices i, j and k of triangle e, and $x_{ij} = x_j - x_i$. The symbols ^ and ~ denote vectors and matrices respectively.

Returning to the variational statement, equation (4.30), the steps taken to transform the time-dependent portion into global matrix form (a form analogous to matrix [CAP] of equation (4.28)) are shown in detail. Considering equation (4.30) term by term and assuming constant properties over each element, the time-dependent portion

may be written as

$$V\, S_t = \frac{\rho^{(e)} C_p^{(e)}}{2} \int\int \frac{\partial (t^{(e)2})}{\partial \theta}\, dx\, dy. \tag{4.36}$$

Utilizing Leibnitz' rule [4] the operator may be withdrawn from the integrand, thus

$$V\, S_t = \frac{\rho^{(e)} C_p^{(e)}}{2} \frac{d}{d\theta} \int\int t^{(e)2}\, dx\, dy. \tag{4.37}$$

Inserting equation (4.31) for the scalar $t^{(e)}$,

$$V\, S_t^{(e)} = \frac{\rho^{(e)} C_p^{(e)}}{2} \frac{d}{d\theta} \int\int (\hat{P}^T \tilde{R}^{(e)} \hat{t}^{(e)})^2\, dx\, dy. \tag{4.38}$$

Differentiating with respect to the vector of nodal points, $\hat{t}^{(e)}$, equation (4.38) becomes

$$\frac{dVS_t^{(e)}}{d\hat{t}^{(e)}} = \rho^{(e)}\, C_p^{(e)} \frac{d}{d\theta} \int\int \hat{P}^T\, \tilde{R}^{(e)}\, \hat{t}^{(e)} (\hat{P}^T \tilde{R}^{(e)})^T dx\, dy. \tag{4.39}$$

Observing that $\hat{P}^T \tilde{R}^{(e)} \hat{t}^{(e)}$ is a scalar quantity, the order of multiplication may be reversed and written.

$$\frac{dVS_t^{(e)}}{d\hat{t}^{(e)}} = \rho^{(e)} C_p^{(e)} \frac{d}{d\theta} \int\int \tilde{R}^{(e)T}\, \hat{P}\, \hat{P}^T\, \tilde{R}^{(e)}\, \hat{t}^{(e)}\, dxdy. \tag{4.40}$$

$\tilde{R}^{(e)}$ and $\hat{t}^{(e)}$, equations (4.33) and (4.35), are each independent of the variables of integration, thus they are withdrawn from the

integrand. Taking the derivative with respect to time,

$$\frac{dVS_t^{(e)}}{d\hat{t}^{(e)}} = \rho^{(e)} C_p^{(e)} R^{(e)T} \int\int \hat{P}\,\hat{P}^T \, dxdy \, \tilde{R}^{(e)} \dot{\hat{t}}^{(e)} \tag{4.41}$$

where $\dot{\hat{t}}^{(e)}$ denotes the time derivative of $\hat{t}^{(e)}$. Carrying out the vector multiplication within the integrand, equation (4.41) may be rewritten as

$$\frac{dVS_t^{(e)}}{d\hat{t}^{(e)}} = \rho^{(e)} \, C_p^{(e)} \, \tilde{R}^{(e)T} \int\int \begin{bmatrix} 1 & x & y \\ x & x^2 & xy \\ y & xy & y^2 \end{bmatrix} dxdy \, \tilde{R}^{(e)} \dot{\hat{t}}^{(e)}. \tag{4.42}$$

Recognizing the physical significance of the nine separate integrations that are indicated in equation (4.42), it may be written that

$$\frac{dVS_t^{(e)}}{d\hat{t}^{(e)}} = \rho^{(e)} C_p^{(e)} \, \hat{R}^{(e)T} \begin{bmatrix} 1 & \bar{x} & \bar{y} \\ \bar{x} & I_y/A^{(e)} & P_{xy}/A^{(e)} \\ \bar{y} & P_{xy}/A^{(e)} & I_x/A^{(e)} \end{bmatrix} \tilde{R}^{(e)} \dot{\hat{t}}^{(e)} A^{(e)} \tag{4.43}$$

where $A^{(e)}$ is the area of triangular element e, and $\bar{x}$ and $\bar{y}$ are the x and y coordinates of its centroid. I_x, I_y, and P_{xy} are the respective second moments and product of inertia of element e about the axes x and y, the main Cartesian system chosen to represent the pressure vessel (see Fig. 4.4). Because most texts list formulas for moments and products of inertia for triangles about a pair of orthogonal axes, one of which is always parallel to a side [18], it becomes necessary to use the parallel axis theorem

to shift the moments and products of inertia to the axes of the vessel. For elements within the hemispherical region, the use of Mohr's Circle is required in addition to the parallel axis theorem to rotate the axes, about which the products and moments of inertia were calculated (see Fig. 4.4), into coincidence with the main coordinate system of the pressure vessel. The parallel axis theorem and rotation formulas are

$$I_y^{(e)} = I_{vcg}^{(e)} + \bar{x}^2 A^{(e)}, \tag{4.44}$$

$$I_x^{(e)} = I_{ucg}^{(e)} + \bar{y}^2 A^{(e)}, \tag{4.45}$$

$$P_{xy}^{(e)} = P_{uvcg}^{(e)} + x\,\bar{y}\,\bar{A}^{(e)}, \tag{4.46}$$

$$I_x^{(e)} = \frac{I_u^{(e)} + I_v^{(e)}}{2} + \frac{I_u^{(e)} - I_v^{(e)}}{2} \cos 2\psi - P_{uv}^{(e)} \sin 2\psi, \tag{4.47}$$

$$I_y^{(e)} = \frac{I_u^{(e)} + I_v^{(e)}}{2} - \frac{I_u^{(e)} - I_v^{(e)}}{2} \cos 2\psi + P_{uv}^{(e)} \sin 2\psi, \tag{4.48}$$

$$P_{xy}^{(e)} = \frac{I_u^{(e)} - I_v^{(e)}}{2} \sin 2\psi + P_{uv} \cos 2\psi. \tag{4.49}$$

ψ is the angle of rotation in the hemispherical region. After adding the contributions from each element, thus building the global capacitance matrix, the final set of equations is written in matrix form as

$$[CAP]\ \{\frac{dT}{d\theta}\} + [CON]\ \{T\} = \{0\}. \tag{4.50}$$

The actual temperature is expressed by

$$\{t\} = \{T\} + \{T_\infty\} \tag{4.51}$$

where T_∞ is the coolant water temperature, assumed constant. Both [CAP] and [CON] of equation (4.50) are pentadiagonal and symmetric.

4.4 Mathematical Solution

Both approaches have reduced the governing partial differential equation to a set of simultaneous, first order, linear, differential equations. The equations will now be solved analytically in time. Taking the finite difference set as an example, equation (4.28), a K x K set, is rewritten

$$[CAP]\ \{\frac{dT}{d\Theta}\} = [CON]\ \{T\}. \tag{4.52}$$

Premultiplying both sides of equation (4.51) by $[CAP]^{-1}$,

$$\{\frac{dT}{d\Theta}\} = [CAP]^{-1}\ [CON]\ \{T\}. \tag{4.53}$$

Defining a linear transformation

$$\{T\} = [VE]\ \{TE\} \tag{4.54}$$

where

$$[CAP]^{-1}\ [CON]\ \{VE(J)\} = \lambda(J)\ \{VE(J)\},\ J=1,2.....K, \tag{4.55}$$

and where $\lambda(J)$ is the Jth eigenvalue of $[CAP]^{-1}$ [CON]. Substituting

equation (4.54) into equation (4.53) gives

$$[VE]\ \{\frac{dTE}{d\Theta}\} = [CAP]^{-1}\ [CON]\ [VE]\ \{TE\}. \tag{4.56}$$

Premultiplying by $[VE]^{-1}$ uncouples the set of equations.

$$\{\frac{dTE}{d\Theta}\} = [\lambda]\ \{TE\}. \tag{4.57}$$

The above equation for the transformed temperatures may be written in alternate form as

$$\frac{dTE(J)}{d\Theta} = \lambda(J)TE(J), \qquad J = 1,2,.....K \tag{4.58}$$

whose solutions are

$$TE(J) = TE_o(J)\ \exp\ (\lambda(J)\Theta), \qquad J = 1,2,.....K. \tag{4.59}$$

In the above, $TE_o(J)$ is the Jth element of $\{TE_o\}$, the transformed initial condition determined from

$$[VE]\ \{TE_o\} = \{t_o\} - \{T_\infty\} \tag{4.60}$$

where $\{t_o\}$ is the vector of actual initial conditions. Actual temperatures at any time Θ are expressed by eliminating $\{TE\}$ from equation (4.54) by substitution of the vector form of equation (4.59) followed by insertion of equation (4.54) into equation (4.51), thereby eliminating $\{T\}$ and resulting in

$$\{t\} = [VE]\ \{TE_o\ \exp(\lambda\Theta)\} + \{T_\infty\}. \tag{4.61}$$

To take the effects of local boiling heat transfer into consideration, the transient solution is divided into three time intervals. After the steady-state profile has been computed, the temperatures of the wetted nodes are instantaneously changed to the saturation temperature of the coolant.* During time interval $\Delta\Theta$, we assume constant temperature wetted nodes. The interval terminates when the following equation is satisfied:

$$(h_c + k_1/\Delta r_1) \sum_{J=1}^{K} VE(M,J)\ TE_o(J)\ \exp\ (\lambda(J)\ \Delta\Theta_1) =$$

$$k_1/\Delta r_1 \sum_{J=1}^{K} VE(N_1J)\ TE_o(J)\ \exp\ (\lambda(J)\ \Delta\Theta_1), \tag{4.62}$$

where VE(M,J) and VE(N,J) are the Jth elements of rows M and N of [VE], the matrix of eigenvectors. Rows M and N designate a wetted node and its radial neighbor near the bottom of the cylindrical section, h_c is the forced convection film coefficient for the cylindrical region, $TE_o(J)$ is the Jth element of the transformed initial condition vector (steady-state temperature profile with surface nodes set to the saturation temperature). Matrix [VE] and

*To verify this assumption, the time required for a node at the beltline to cool to the saturation temperature was calculated. The time was determined to be less than 0.02 second, and the effect on radially neighboring nodes was, at most, 0.03 degree. The neighboring nodes are at the clad-vessel interface, Δr_1 = 0.00476 m.

eigenvalues $\lambda(J)$ reflect a constant surface temperature boundary condition. Condition (4.62) is solved for $\Delta\theta$, by trial and error and expresses the time needed for the radial temperature gradient of the cylindrical section to attenuate to such an extent that the heat removed from the wetted nodes by forced convection (vice nucleate boiling) is sufficient to cause their temperature to decrease from that point on in time. Once $\Delta\theta_1$ is determined, the entire solution is advanced in time by the same amount. The profile existing in the pressure vessel at $\theta = \Delta\theta_1$ becomes the initial condition for time interval $\Delta\theta_2$.

In a manner analogous to that used to calculate $\Delta\theta_1$, $\Delta\theta_2$ is sought which is the additional time the hemispherical section is to be held at constant surface temperature once the cylindrical section has begun cooling by forced convection. Expressed as an equation to be solved for $\Delta\theta_2$,

$$(h_s + k_1/\Delta r_1) \sum_{J=1}^{K} VE(M,J)\ TE_o(J)(\exp\ (\lambda(J)(\Delta\theta_1 + \Delta\theta_2)) =$$

$$k_1/\Delta r_1 \sum_{J=1}^{K} VE\ (N,\ J)\ TE_o(J)\ \exp(\lambda(J)(\Delta\theta_1 + \Delta\theta_2)). \qquad (4.63)$$

In equation (4.62) $TE_o(J)$ is the Jth element of the transformed temperatures existing at the end of interval $\Delta\theta_1$. Matrix [VE] and eigenvalues $\lambda(J)$ reflect forced convection boundary conditions in the cylindrical region and constant wetted surface temperature in

the hemispherical region. VE (M,J) and VE (N,J) are the Jth elements of rows M and N of matrix [VE]. M and N designate a wetted node and its radial neighbor, which is at the clad-vessel interface of the hemispherical region, respectively. Trial and error solution of equation (4.63) yields $\Delta\Theta$ which then is used to move the entire solution ahead in time to the beginning of $\Delta\Theta_3$, the final time interval in which forced convection is assumed in both upper and lower sections.

4.5 Results

The particular case considered [1] involved a vessel having the same dimensions as those used in previous chapters. The initial profile was calculated using a coolant temperature of 290.83°C with film coefficients of 1988.3 and 1491.3 W/m^2-°C for the upper and lower sections respectively. During the transient, the coolant temperature was taken as a conservative 4.444°C. Local boiling film coefficients for both sections were 397210 W/m^2-°C [10]. Once it was determined that boiling subsided, forced convection film coefficients were assumed to be 896.57 and 672.43 W/m^2-°C for the upper and lower sections respectively [19]. The saturation temperature of the coolant is assumed to be 138.33°C which corresponds to a static pressure of roughly 24130 N/m^2.

The upper number of each pair of entries in Tables 4.1 through 4.5 are the temperatures at respective times of 0.00, 1.44, 2.40, 10.0 and 30.0 minutes following initiation of the transient. The

Table 4.1 Initial profiles of reactor vessel, θ = 0.0 min, h_c = 1988.3, h_s = 1491.2 W/m^2-°C, q'''_{oc} = 258.570, q'''_{os} = 51715 W/m^3, b = clad-vessel interface.

Axial Location	$\bar{r}$ = 0.0	$\bar{r}$ = b	$\bar{r}$ = .20	$\bar{r}$ = .40	$\bar{r}$ = .60	$\bar{r}$ = .80	$\bar{r}$ = 1.0
h = 3.048	295.37	297.81	301.99	303.23	303.59	303.69	303.70
	295.38	299.93	303.59	304.68	304.99	305.08	305.09
h = 1.829	295.37	297.81	301.99	303.23	303.59	303.69	303.70
	295.38	299.93	303.59	304.68	304.99	305.08	305.09
h = .6096	295.33	297.74	301.86	303.04	303.36	303.43	303.44
	295.33	299.84	303.42	304.44	304.70	304.76	304.76
h = .3048	295.16	297.47	301.26	302.21	302.36	302.34	302.32
	295.14	299.42	302.66	303.43	303.53	303.49	303.46
h = 0.0 ψ = 0°	293.06	294.25	296.33	296.97	297.18	297.25	297.27
	293.07	295.31	297.14	297.71	297.90	297.97	297.98
ψ = 9°	291.16	291.29	291.66	291.90	292.06	292.14	292.17
	291.18	291.46	291.84	291.55	292.28	292.37	292.41
ψ = 18°	290.96	291.02	291.13	291.18	291.22	291.24	291.24
	290.97	291.08	291.19	291.25	291.29	291.31	291.31
ψ = 54°	290.93	290.17	291.03	291.06	291.06	291.06	291.06
	290.93	291.00	291.06	291.08	291.08	291.08	291.08
ψ = 72°	290.93	290.97	291.03	291.06	291.06	291.06	291.06
	280.93	291.00	291.06	291.08	291.08	291.08	291.08

Table 4.2 Temperature profiles of reactor vessel, Θ = 1.44 min, b = clad-vessel interface.

Axial Location	$\bar{r}$ = 0.0	$\bar{r}$ = b	$\bar{r}$ = .20	$\bar{r}$ = .40	$\bar{r}$ = .60	$\bar{r}$ = .80	$\bar{r}$ = 1.0
h = 3.048	138.33	172.80	269.28	297.42	302.76	303.56	303.66
	138.33	207.04	281.67	302.62	304.45	304.99	305.06
h = 1.829	138.33	172.80	269.28	297.42	302.76	303.56	303.66
	138.33	207.04	281.67	302.62	304.45	304.99	305.06
h = .6096	138.33	172.77	269.16	297.24	302.52	303.31	303.40
	138.33	206.97	281.51	300.72	304.16	304.67	305.28
h = .3048	138.33	172.64	268.60	296.41	301.53	302.21	302.28
	138.33	206.67	280.78	299.72	302.99	303.40	303.43
h = 0.0	138.33	171.87	264.96	291.59	296.46	297.16	297.24
ψ = 0°	138.33	204.83	276.32	294.34	297.46	297.91	297.97
ψ = 9°	138.33	171.06	261.42	286.88	291.44	292.08	292.17
	138.33	203.03	271.97	289.03	291.92	292.34	292.40
ψ = 18°	138.33	170.94	260.94	286.17	290.60	291.17	291.23
	138.33	202.77	271.34	288.17	290.92	291.27	291.31
ψ = 54°	138.33	170.92	260.85	286.04	290.44	291.00	291.05
	138.33	202.72	271.22	288.00	290.72	291.05	291.08
ψ = 72°	138.33	170.92	260.85	286.04	290.44	291.00	291.05
	138.33	202.72	271.22	288.00	290.72	291.05	291.08

Table 4.3 Temperature profiles of reactor vessel, Θ = 2.40, 2.28 min, b = clad-vessel interface.

Axial Location	$\bar{r}$ = 0.0	$\bar{r}$ = b	$\bar{r}$ = .20	$\bar{r}$ = .40	$\bar{r}$ = .60	$\bar{r}$ = .80	$\bar{r}$ = 1.0
h = 3.048	129.38	161.32	250.72	289.27	300.60	303.13	303.52
	128.89	191.18	267.36	295.74	303.21	304.75	304.98
h = 1.829	129.38	161.32	250.72	289.27	300.60	303.13	303.52
	128.89	191.18	267.36	295.74	303.21	304.75	304.98
h = .6096	129.34	161.27	250.59	289.09	300.37	302.87	303.26
	128.84	191.09	267.19	295.50	302.92	304.43	304.65
h = .3048	129.15	161.02	250.04	288.27	299.38	301.78	302.13
	128.61	190.73	266.48	294.52	301.75	303.16	303.35
h = 0.0	128.19	159.78	246.94	283.84	294.47	296.77	297.12
ψ = 0°	127.38	188.78	262.53	289.42	296.32	297.71	297.91
ψ = 9°	138.33	164.37	244.54	279.52	289.57	291.74	292.07
	138.33	190.39	258.96	284.39	290.88	292.17	292.35
ψ = 18°	138.33	164.25	244.09	278.82	288.74	290.83	291.13
	138.33	190.16	258.36	283.55	289.89	291.09	274.59
ψ = 54°	138.33	164.25	244.01	278.69	288.58	290.66	290.95
	138.33	190.11	258.23	283.38	289.68	290.87	291.03
ψ = 72°	138.33	164.25	244.01	278.69	288.58	290.66	290.95
	138.33	190.11	258.23	283.38	289.68	290.87	291.03

Table 4.4 Temperature profiles of reactor vessel, Θ = 10 min, h_c = 896.57, h_s = 672.43 W/m^2-°C, b = clad-vessel interface.

Axial Location	$\bar{r}$ = 0.0	$\bar{r}$ = b	$\bar{r}$ = .20	$\bar{r}$ = .40	$\bar{r}$ = .60	$\bar{r}$ = .80	$\bar{r}$ = 1.0
h = 3.048	89.91	111.92	180.50	231.62	264.72	282.44	287.89
	87.98	130.69	195.52	242.50	272.11	287.60	292.29
h = 1.829	89.91	111.92	180.50	231.62	264.72	282.44	287.89
	87.98	130.69	195.52	242.50	272.11	287.60	292.29
h = .6096	89.84	111.83	180.36	231.43	264.49	282.19	287.63
	87.90	130.57	195.33	242.26	271.82	287.28	292.22
h = .3048	89.57	111.49	179.79	230.65	263.55	281.14	286.55
	87.60	130.12	194.62	241.31	270.70	286.05	290.70
h = 0.0	89.17	110.97	178.49	228.31	260.29	277.27	282.46
ψ = 0°	87.00	129.17	192.74	238.36	266.84	281.62	286.07
ψ = 9°	106.53	126.20	186.57	230.83	259.22	274.31	278.92
	104.08	142.13	198.97	239.51	264.77	277.88	281.83
ψ = 18°	106.42	126.06	186.26	230.29	258.49	273.47	278.04
	103.90	141.87	198.50	238.80	263.88	276.87	280.78
ψ = 54°	106.39	125.99	186.16	230.16	258.34	273.29	277.86
	103.84	141.78	198.37	238.62	263.68	276.65	280.55
ψ = 72°	106.37	125.99	186.16	230.76	258.34	273.29	277.86
	103.84	141.78	198.37	238.62	263.68	276.65	280.55

Table 4.5 Temperature profiles of reactor vessel, Θ = 30 min, b = clad-vessel interface.

Axial Location	$\bar{r}$ = 0.0	$\bar{r}$ = b	$\bar{r}$ = .20	$\bar{r}$ = .40	$\bar{r}$ = .60	$\bar{r}$ = .80	$\bar{r}$ = 1.0
h = 3.048	57.72	71.47	115.86	152.88	180.58	197.65	203.38
	57.78	85.21	128.91	165.03	203.00	208.37	213.89
h = 1.829	57.72	71.47	115.86	152.88	180.58	197.65	203.38
	57.78	85.21	128.91	165.03	203.00	208.37	213.89
h = .6096	57.65	71.39	115.72	152.69	172.02	197.41	203.13
	57.71	85.09	128.72	164.79	191.61	208.06	213.57
h = .3048	57.48	71.17	115.35	152.18	179.73	196.70	202.41
	57.49	84.77	145.99	164.12	190.81	207.17	212.66
h = 0.0	57.98	71.79	116.07	152.63	179.76	196.35	201.89
ψ = 0°	57.83	85.24	128.62	164.14	190.33	206.28	211.60
ψ = 9°	72.28	85.38	127.09	161.17	186.24	204.47	206.53
	71.89	97.79	138.48	171.48	195.62	210.22	215.06
ψ = 18°	72.42	85.55	127.26	161.25	186.21	201.34	206.37
	71.94	97.86	138.50	171.37	195.37	209.88	214.68
ψ = 54°	72.37	85.49	127.18	161.14	186.07	201.20	206.22
	71.88	97.77	138.37	171.22	195.19	209.68	214.48
ψ = 72°	72.37	85.49	127.18	161.14	186.07	201.20	206.22
	71.88	97.77	138.37	171.22	195.19	209.68	214.48

lower number of each pair gives the same information for a vessel with a 0.00953 m clad at times of 0.00, 1.44, 2.28, 10.0, and 30.0 minutes respectively. Columns of the tables pinpoint axial locations while row headings designate normalized radial positions. Tables 4.2 and 4.3 show profiles at the end of time intervals $\Delta\theta_1$ and $\Delta\theta_2$ respectively.

Inspecting the tables reveals axial heat conduction is slight and is concentrated about the vicinity of the common boundary of the upper and lower sections for a cladding of 0.00476 m. The effect of doubling the cladding is significant. The increase in thickness causes reductions in overall temperature gradients within the cylindrical wall at the end of time intervals $\Delta\theta_1$, $\Delta\theta_2$, 10.0, 30.0 minutes of 25%, 20%, 9%, and 2% respectively. This reduction in the radial temperature gradient can easily be seen in Fig. 4.5 which shows the maximum gradient occurring approximately 11 minutes after initiation of the transient. As anticipated, axial heat conduction increases with increasing cladding thickness. Although not shown by the tables, small axial temperature gradients extend as far as 1.219 m above the common boundary of the upper and lower halves, whereas with a 0.00476 cladding, the gradients extend only as far as 0.6096 m.

4.6 Nomenclature

A_r, A_z, A_ψ = areas through which heat enters volume ΔV, subscripts denote direction of normal to area

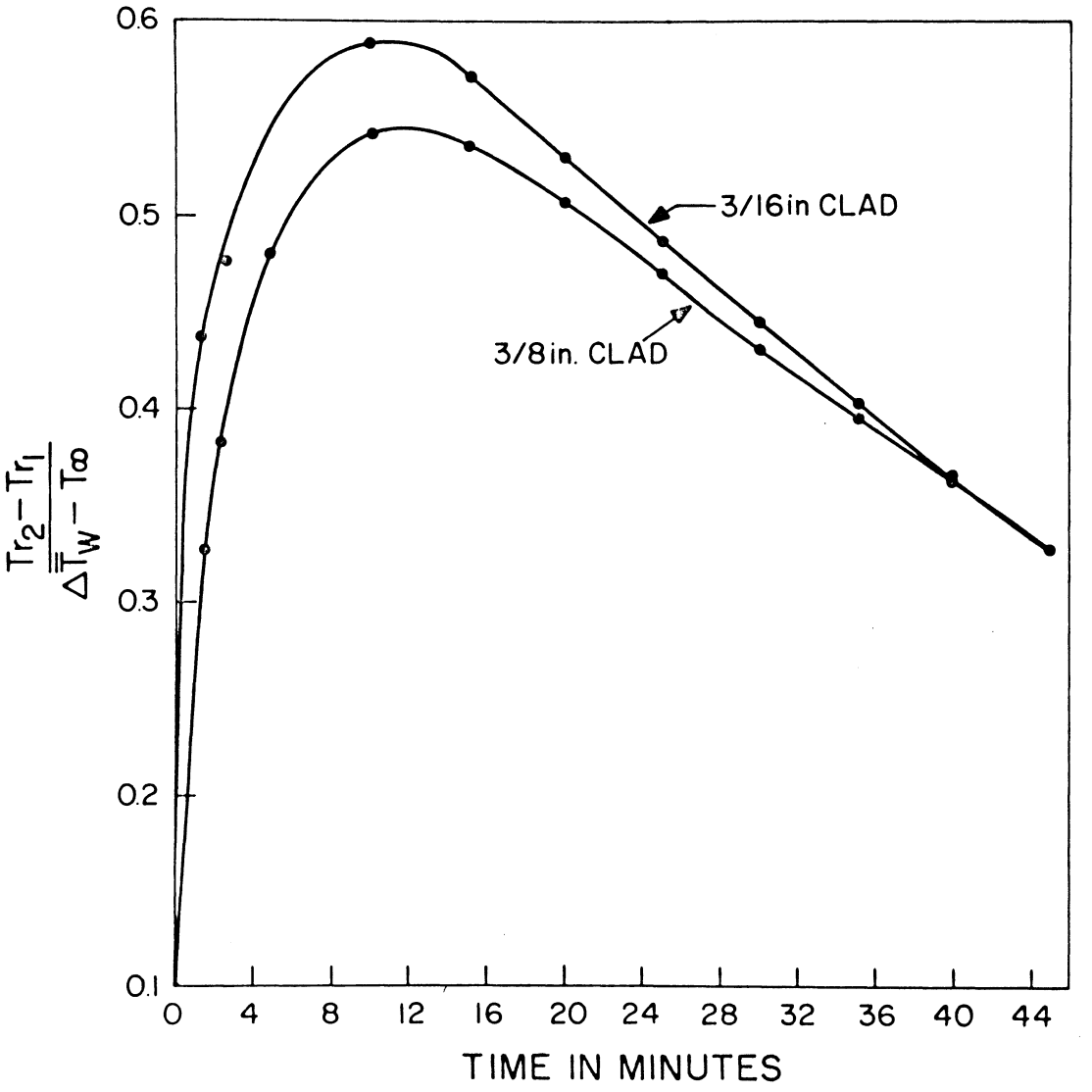

Figure 4.5 Dimensionless temperature difference between insulated outer wall and clad-wall interface for long periods of time for two thicknesses of cladding.

$A^{(e)}$ = area of a finite element

[CAP] = capacitance matrix, K x K

[CON] = conductance matrix, K x K

C_{p_1}, C_{p_2} = specific heats of clad and wall regions respectively

D = a scalar defined by equation (4.34)

I, J = indices of matrices or vectors

i, j, k = vertices of triangular elements

K = total number of equations (and nodes/vertices) describing pressure vessel

k_1, k_2 = conductivities of clad and wall regions respectively

q'''_{oc}, q'''_{os} = internal heat generation rates of upper and lower sections of vessel per unit time and volume

r = radial coordinate

$\bar{r}$ = normalized radial coordinate

r_0, r_1, r_2 = radii of clad-water interface, clad-wall interface

{T} = vector of actual temperatures minus coolant temperature defined by equations (4.29) and (4.51)

{t} = vector of actual temperatures defined by equations (4.29) and (4.51)

$\{t_o\}$ = vector of actual initial conditions for any time interval of solution

$\hat{t}^{(e)}$ = vector defined by equation (4.35)

{TE} = vector of transformed temperatures defined by equation (4.54)

$\{TE_o\}$ = vector of transformed initial conditions for any time interval defined by equation (4.60)

u, v = Cartesian axis of each element with origin located at centroid and u parallel to radial direction

[VE] = matrix of eigenvectors defined by equation (4.55)

VS = variational statement of transient heat conduction equation

VS_t = time-dependent portion of variational statement

x, y = Cartesian coordinate system of pressure vessel

z = vertical coordinate of cylindrical region

Δr_1, Δr_2 = radial increments of clad and wall regions respectively

ΔV_1, ΔV_2 = volumes of nodes in clad and wall regions respectively

$\Delta\theta_1, \Delta\theta_2, \Delta\theta_3$ = time intervals of solution, each reflecting different boundary conditions

θ = time variable

λ = eigenvalue

ψ = angular variable in hemispherical region

V. Concluding Remarks

5.1 Methods

It has been shown that separation of variables can be applied to the Poisson equations describing heat flow in a region composed of two differing geometries, each of which is bimetallic and where the inhomogeneous terms of the equations are functions of the same independent variable as are the eigenfunctions. Clearly, the technique will also work for a composite vessel made of more than two different materials as well as for the less complicated case of constant heat generation. For the case of zero heat generation, the set of equations (3.72) becomes homogeneous, thus the expansion coefficients are all zero, indicating a flat temperature profile, which is precisely what physical reasoning concludes.

As with most analytical solutions, computation time is short compared to purely numerical solutions of comparable accuracy. However, the situations to which analytical solutions can be applied are few and highly idealized. The closed form solution derived in Chapter III provides an instance where such a solution can describe a physical situation that has not been unduly altered to conform to the requirements of Sturm-Liouville theory.

The hybrid method as used in Chapter IV can be advantageous compared to purely numerical methods for the following reasons:

1. Nodes and elements may be positioned without regard to stability criteria and time step size.

2. Roundoff errors caused by time-stepping the solution are eliminated.
3. Time derivatives are not approximated.
4. Computer routines for efficient eigenanalysis are readily available, thus the method is convenient to use.

Disadvantages of the method may be summarized as follows:

1. Matrix methods of the type used cannot be applied to non-linear (radiation) boundary conditions.
2. Time-dependent boundary conditions must be satisfactorily represented by a few characteristic values, otherwise computation time becomes excessive.
3. The method requires more storage than do purely numerical techniques.
4. For storage and computational reasons, the method is limited to applications which produce symmetric matrices in eqs. 4.28 and 4.50.

The finite difference solution was found superior to the finite element solution for the problem attacked herein. There are several reasons, and they are enumerated below.

1. The accuracy and stability of the finite element technique are sensitive to the aspect ratio of the triangular elements which, due to the height of a pressure vessel, is large if a node is placed at either radial extremity of the cladding. While the accuracy of a finite difference solution is also affected by a coarse nodal network, the effect appears less pronounced and no oscillations near

boundaries are caused as with the finite element solution.

2. The finite element set of equations (4.50) includes the presence of more than one time derivative per equation. This nearly doubles computation time.
3. Stable oscillations are inherent at early times in the solution when more than one time derivative is present per equation. G. E. Myers [15] suggests setting all off-diagonal derivatives to zero after adding their contribution to the main diagonal on a row by row basis. The scheme was implemented but produced unsatisfactory results.

5.2 Numerical Results

The steady-state solution in Chapter III, in conflict with the solution in the previous chapter, demonstrates that maximum temperatures do not necessarily occur at the outer boundary of the vessel, particularly in proximity to the mutual boundary of the two halves. With a 0.00953 m cladding, the point of inflection extends 1.219 m above the mutual boundary.

The steady-state profile of the one-dimensional solution is in good agreement with the two-dimensional solution for positions near the top of the cylindrical half of the vessel where heat flow is essentially radial. Similarly, the two-dimensional transient solution also produced results in close agreement with those of the one-dimensional transient solution when the boundary conditions of the former were altered to conform to those used in the latter. A 1.1-1.7°C

temperature difference in the results does exist, but it is felt the slight difference is due to zero heat generation used in the transient portion of the two-dimensional analysis for $\Theta > 0$. Furthermore, altering the physical dimensions and boundary conditions to conform to those used in reference [19], an experimental investigation, produced results which differed by only a few per cent in both the maximum temperature gradient in the wall and the time at which it occurred.

It is apparent from the results reported herein that the lower hemispherical shell does little to attenuate radial temperature gradients in the upper region. It would appear that a one-dimensional analysis, providing it reflects bimetallic construction, time-varying film coefficients, and an initial profile based on internal heat generation considerations, should yield definitive results for much of the cylindrical region, and in addition, yield conservative results if applied to the remainder of the pressure vessel, the hemispherical section included (assuming similar physical dimensions). It may also be concluded from the results that the temperature gradients at long time intervals after the loss of coolant accident are critically dependent on the cladding thickness. Thus the cladding may be considered an insulating region, protecting the carbon steel portion of the vessel wall from the sharp temperature gradients which could be induced by emergency cooling.

References

1. Gloudemans, J. R., Reactor Vessel Thermal Shock, Internal Memorandum, Babcock and Wilcox Company, Lynchburg, Va., May (1975).

2. Ölcer, N. Y., Quarterly Applied Math, Vol. 26, (1968), pp. 355-371.

3. Yeh, H. C., Nuclear Engineering and Design, Vol. 32, (1975), pp. 85-104.

4. Hildebrand, F. B., Advanced Calculus for Applications, Prentice-Hall, Englewood Cliffs, New Jersey, (1962), pp. 206-213.

5. Tittle, C. W., Journal of Applied Physics, Vol. 36, (1965), pp. 1486-1488.

6. Giere, A. C., American Journal of Physics, Vol. 36, (1968), pp. 994-1000.

7. Özisik, M. N., Boundary Value Problems of Heat Conduction, International Textbook Company, Scranton Pennsylvania, (1968), pp. 273-275.

8. Yeh, H. C., Nuclear Engineering and Design, Vol. 36, (1976), pp. 139-157.

9. Nijsing, R., and W. Eifler, Nuclear Engineering and Design, Vol. 32, (1975), pp. 208-220.

10. Holman, J. P., Heat Transfer, McGraw-Hill, New York, (1972), pp. 299-320.

11. Rohsenow, W. M., and J. P. Hartnett, Handbook of Heat Transfer, McGraw-Hill, New York, (1973), pp.

12. Burck, Von E., W. Hufschmidt, and E. de Clercq, Atomkerenergie, Vol. 21, (1973), pp. 127-135.

13. West, J. T. III, Removal-Diffusion Theory vs. Transport Theory in Shield Design: SABINE-ANISN Comparison, Proc. 20th Annual Conf. of the ANS, Philadelphia, Pa., (1974).

14. El Wakil, M. M., Nuclear Heat Transport, International Textbook Company, Scranton, Pennsylvania, (1971), pp. 200-230.

15. Myers, G. E., Analytical Methods in Conduction Heat Transfer, McGraw-Hill, New York, (1971).

16. Abramowitz, M., and I. A. Stegun, Handbook of Mathematical Functions, Dover, New York, (1972), pp. 358-433.

17. Byerly, W. E., An Elementary Treatise on Fourier's Series and Spherical, Cylindrical, and Ellipsoidal Harmonics, Ginn and Company, Boston, (1893), p. 193.

18. Beer, F. P., and E. R. Johnston, Jr., Vector Mechanics for Engineers: Statics and Dynamics, McGraw-Hill, New York, (1962), pp. 321-348.

19. Crane, R. A., Loss of Coolant Accident, Internal Memorandum, Babcock and Wilcox Company, Lynchburg, Va., March, (1974).

The vita has been removed from the scanned document

A THEORETICAL ANALYSIS OF THE TEMPERATURE RESPONSE IN A BIMETALLIC, COMPOSITE GEOMETRY, NUCLEAR REACTOR PRESSURE VESSEL UNDERGOING A LOSS-OF-COOLANT ACCIDENT

by

Lawrence A. Coppari

(ABSTRACT)

This work addresses the problem of thermal shock in a light water cooled nuclear reactor undergoing emergency cooling following a hypothetical loss of coolant accident. Portions of this work provide novel approaches to heat conduction problems. Moreover, the scope of this analysis is broader than that which is currently sought in industry.

In the first solution to the problem, the general heat conduction equation in one dimension is solved analytically by the method of variation of parameters. The domain of the solution is the radius of the bimetallic, upper cylindrical region of the pressure vessel. The solution considers spatially and time-varying internal heat generation.

The two-dimensional analysis of the problem is begun next. Assuming axisymmetric heat conduction, the steady-state profile, which exists in the pressure vessel at the time the loss of coolant accident occurs, is determined by separation of variables. This analysis is innovative because of the following: the solution is composed of four analytical solutions of the two-dimensional Poisson equation, two in cylindrical coordinates and two in the spherical coordinate

system, each pair spanning media having different thermal properties. The inhomogeneous heat generation term in each of the four regions is a function of an independent variable. The eigensolutions derived for the cylindrical section are joined along the mutual boundary to the eigensolutions of the spherical regions by first imposing continuity constraints on the dependent variables and their first derivatives followed by an exploitation of the orthogonal nature of the eigensolutions. Contrary to one-dimensional results, a two-dimensional analysis indicates that maximum temperatures do not necessarily occur at the outer insulated boundary of the pressure vessel. The results of this analysis are verified by numerical techniques and are used as the initial conditions for the two-dimensional, transient analysis that follows.

The transient analysis is formulated by both finite difference and finite element techniques for the purposes of method comparison and verification of results. Each technique results in a set of linear, first order, ordinary differential equations which are solved exactly in time by matrix methods instead of the usual time-stepping, numerical procedures. The merits and demerits of matrix methods used in conjunction with each numerical technique for handling the spatial variables of the problem are enumerated. The analysis considers boiling heat transfer, and results indicate axisymmetric heat flow into the lower hemispherical region has a mitigating effect on radial temperature gradients in only the lower 20% of the cylindrical region. The effect of different clad thicknesses is also discussed.